

# Multielectron Atom Transfer Reactions of Perchlorate and Other Substrates Catalyzed by Rhenium Oxazoline and Thiazoline Complexes: Reaction Kinetics, Mechanisms, and Density Functional Theory Calculations

Lee D. McPherson,<sup>†</sup> Markus Drees,<sup>‡</sup> Saeed I. Khan,<sup>†</sup> Thomas Strassner,<sup>\*,†</sup> and Mahdi M. Abu-Omar<sup>\*,§</sup>

Department of Chemistry and Biochemistry, University of California, Los Angeles, California 90095, Institut für Organische Chemie, TU Dresden, Bergstrasse 66, D-01062 Dresden, Germany, and Department of Chemistry, Purdue University, 560 Oval Drive, West Lafayette, Indiana 47907

Received January 27, 2004

The title complexes, the  $\text{Re}(\text{O})\text{L}_2(\text{Solv})^+$  complexes ( $\text{L} = \text{hoz}$ , 2-(2'-hydroxyphenyl)-2-oxazoline(–) or  $\text{thoz}$ , 2-(2'-hydroxyphenyl)-2-thiazoline(–);  $\text{Solv} = \text{H}_2\text{O}$  or  $\text{CH}_3\text{CN}$ ), are effective catalysts for the following fundamental oxo transfer reaction between closed shell molecules:  $\text{XO} + \text{Y} \rightarrow \text{X} + \text{YO}$ . Among suitable oxygen acceptors (Y's) are organic thioethers and phosphines, and among suitable oxo donors (XO's) are pyridine *N*-oxide (PyO), *t*-BuOOH, and inorganic oxyanions. One of the remarkable features of these catalysts is their high kinetic competency in effecting perchlorate reduction by pure atom transfer. Oxo transfer to rhenium(V) proceeds cleanly to afford the cationic dioxorhenium(VII) complex  $\text{Re}(\text{O})_2\text{L}_2^+$  in a two-step mechanism, rapid substrate (XO) coordination to give the precursor adduct  $\text{cis-Re}^{\text{V}}(\text{O})(\text{OX})\text{L}_2^+$  followed by oxygen atom transfer (OAT) as the rate determining step. Electronic variations with PyO derivatives demonstrated that electron-withdrawing substituents accelerate the rate of  $\text{Re}^{\text{VII}}(\text{O})_2\text{L}_2^+$  formation from the precursor adduct  $\text{cis-Re}^{\text{V}}(\text{O})(\text{OX})\text{L}_2^+$ . The activation parameters for OAT with picoline *N*-oxide and chlorate have been measured; the entropic barrier to oxo transfer is essentially zero. The potential energy surface for the reaction of  $\text{Re}(\text{O})(\text{hoz})_2(\text{OH}_2)^+$  with PyO was defined, and all pertinent intermediates and transition states along the reaction pathway were located by density functional theory (DFT) calculations (B3LYP/6-31G\*). In the second half of the catalytic cycle,  $\text{Re}(\text{O})_2\text{L}_2^+$  reacts with oxygen acceptors (Y's) in second-order reactions with associative transition states. The rate of OAT to substrates spans a remarkable range of  $0.1\text{--}10^6 \text{ L mol}^{-1} \text{ s}^{-1}$ , and the substrate reactivity order is  $\text{Ph}_3\text{P} > \text{dialkyl sulfides} > \text{alkyl aryl sulfides} > \text{Ph}_2\text{S} \sim \text{DMSO}$ , which demonstrates electrophilic oxo transfer. Competing deactivation and inhibitory pathways as well as their relevant kinetics are also reported.

## Introduction

Examples of thermodynamically favorable oxygen atom transfer (OAT) reactions between closed shell organic molecules are plentiful.<sup>1</sup> However, these reactions do not occur under normal and nonforcing conditions. A classic example is sulfoxide disproportionation to sulfide and sulfone

(eq 1). The extremely slow kinetics of this reaction renders sulfoxides stable indefinitely. In contrast, transition metal complexes have been utilized extensively in catalyzing OAT to and from organic compounds.<sup>2,3</sup> Therefore, it is not surprising that enzymes have evolved to employ transition metals in combating the kinetic inertness of OAT reactions of closed shell organic molecules.<sup>4</sup> Of particular interest in this context are the Mo and W containing enzymes such as

\* Authors to whom correspondence should be addressed. E-mail: Thomas.strassner@chemie.tu-dresden.de (T.S.); mabuomar@purdue.edu (M.M.A.-O.).

<sup>†</sup> University of California, Los Angeles.

<sup>‡</sup> TU Dresden.

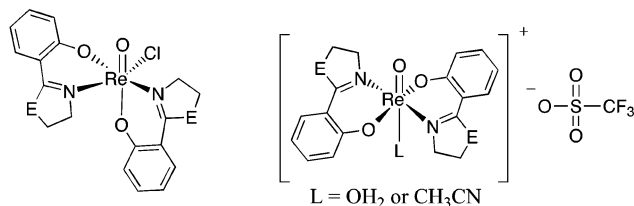
<sup>§</sup> Purdue University.

(1) Holm, R. H.; Donahue, J. P. *Polyhedron* **1993**, *12*, 571–589.

(2) Sheldon, R. A.; Kochi, J. *Metal-Catalyzed Oxidations of Organic Compounds*; Academic Press: New York, 1981.

(3) Collman, J. P.; Zhang, X.; Lee, V. J.; Uffelman, E. S.; Branman, J. I. *Science* **1993**, *261*, 1404–1411.

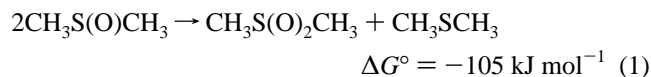
(4) Hille, R. *Chem. Rev.* **1996**, *96*, 2757–2816.



E = O, [Re(O)(hoz)<sub>2</sub>Cl], **1**      E = O, [Re(O)(hoz)<sub>2</sub>(L)]OTf, **2**  
 E = S, [Re(O)(thoz)<sub>2</sub>Cl], **1a**      E = S, [Re(O)(thoz)<sub>2</sub>(L)]OTf, **2a**

**Figure 1.** Rhenium oxazoline and thiozoline catalysts. Abbreviations: hoz = 2-(2'-hydroxyphenyl)-2-oxazoline, thoz = 2-(2'-hydroxyphenyl)-2-thiozoline, and OTf = trifluoromethanesulfonate.

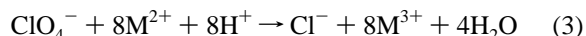
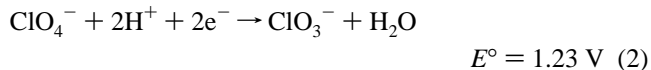
dimethyl sulfoxide (DMSO) reductase, sulfite oxidase, and nitrate reductase.<sup>5–7</sup> The active site Mo or W of these enzymes cycles between the +4 (d<sup>2</sup>) and +6 (d<sup>0</sup>) oxidation states, which are isoelectronic to Re<sup>V</sup> and Re<sup>VII</sup>, respectively. Modeling the active sites of molybdenum and tungsten enzymes has received much attention with a focus on effecting OAT from sulfoxides to tertiary phosphines.<sup>8–13</sup> Nonetheless, most of the known molybdenum model complexes suffer two major drawbacks: (1) sluggish kinetics and (2) deactivation via the facile and irreversible formation of dimeric  $\mu$ -oxo–Mo<sup>V</sup> species.



We have developed a new class of molecular rhenium oxotransferases that contain oxazoline and thiazoline ancillary ligands (Figure 1). The oxazoline binding moiety occurs naturally in the siderophores mycobactin and agrobactin.<sup>14,15</sup> Transition metal complexes of oxazoline are less susceptible to hydrolytic and oxidative degradation than their Schiff base analogues. These rhenium complexes are highly effective in catalyzing OAT from several oxo donors to organic thioethers via a mechanism that involves Re<sup>V</sup>(O) in the reduced state and Re<sup>VII</sup>(O)<sub>2</sub> in the oxidized state. One of the remarkable attributes of the oxazoline rhenium complexes is their unsurpassed ability to catalyze perchlorate reduction all the way to chloride by pure atom transfer, which is extremely difficult kinetically, at record rates under mild conditions.<sup>16</sup>

- (5) Enemark, J. H.; Young, C. G. *Adv. Inorg. Chem.* **1993**, *40*, 1–88.
- (6) Schultz, B. E.; Hille, R.; Holm, R. H. *J. Am. Chem. Soc.* **1995**, *117*, 827–828.
- (7) Young, C. G. In *Biomimetic Oxidations Catalyzed by Transition Metal Complexes*; Meunier, B., Ed.; Imperial College Press: London, 2000, pp 415–459.
- (8) Caradonna, J. P.; Reddy, P. R.; Holm, R. H. *J. Am. Chem. Soc.* **1988**, *110*, 2139–2144.
- (9) Schultz, B. E.; Holm, R. H. *Inorg. Chem.* **1993**, *32*, 4244–4248.
- (10) Laughlin, L. J.; Young, C. G. *Inorg. Chem.* **1996**, *35*, 1050–1058.
- (11) Xiao, Z.; Bruck, M. A.; Enemark, J. H.; Young, C. G.; Wedd, A. G. *Inorg. Chem.* **1996**, *35*, 7508–7515.
- (12) Smith, P. D.; Millar, A. J.; Young, C. G.; Ghosh, A.; Basu, P. *J. Am. Chem. Soc.* **2000**, *122*, 9298–9299.
- (13) Lim, B. S.; Willer, M. W.; Holm, R. H. *J. Am. Chem. Soc.* **2001**, *123*, 8343–8349.
- (14) Eng-Wilmot, D. L.; Van der Helm, D. *J. Am. Chem. Soc.* **1980**, *102*, 7719–7725.
- (15) Maurer, P. J.; Miller, M. J. *J. Am. Chem. Soc.* **1983**, *105*, 240–245.
- (16) Abu-Omar, M. M.; McPherson, L. D.; Arias, J.; Béreau, V. M. *Angew. Chem., Int. Ed.* **2000**, *39*, 4310–4313.

Despite the driving force for the reduction of perchlorate to chlorate (eq 2), its reactions in solution are very sluggish because ClO<sub>4</sub><sup>−</sup> is nonlabile and its redox center, Cl<sup>VII</sup>, is shielded by the oxygens.<sup>17,18</sup> Of particular interest is perchlorate's reduction by divalent first-row transition metals (eq 3), which either does not occur in solution under normal conditions or takes place at rates that are tremendously slow.<sup>19–23</sup> The highly reducing Cr<sup>2+</sup>(aq) is stable indefinitely toward perchlorate as long as the latter is free of chlorate impurities.<sup>24,25</sup> Even labile reductants such as Ti<sup>3+</sup> react with perchlorate very slowly.<sup>23</sup> Consequently, perchlorate salts are widely used to adjust ionic strength in kinetics and electrochemical studies.

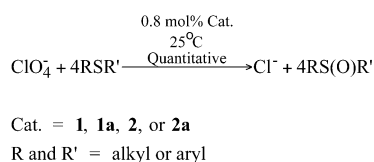


M = 3d metals such as Fe, Cr, Mn, etc.

In 1997, perchlorate was recognized as an environmental contaminant in water supplies in several states in the United States.<sup>26</sup> Perchlorate toxicity stems from its irreversible binding to the thyroid gland inhibiting the production of vital hormones.<sup>27</sup> In addition to its use as a component of air bag inflators and as an additive in lubricating oils and paints, ammonium perchlorate continues to be a major ingredient in propulsion systems both as a solid oxidant when reacted with powdered aluminum as a reducing agent and as an energy booster.<sup>28</sup> Even though the sources of perchlorate in the environment are not always identifiable, given its use in rocket fuel, military and aerospace activities have undergone scrutiny in the past few years.<sup>29</sup> Perchlorate poses serious challenges for remediation due to the high solubility of its salts in both aqueous and organic solvents and due to its kinetic inertness toward reductants in solution. Therefore, typical water treatments such as precipitation, carbon adsorption, and air stripping are not effective.<sup>26</sup> Anion exchange and microbiological reduction of perchlorate have been the dominant areas in remediation research.<sup>30–34</sup> Another ap-

- (17) Taube, H. *ACS Symp. Ser.* **1982**, *198*, 151–171.
- (18) Espenson, J. H. In *Perchlorate in the Environment*; Urbansky, E. T., Ed.; American Chemical Society: Washington, DC, 2000, pp 1–7.
- (19) King, W. R.; Garner, C. S. *J. Phys. Chem.* **1954**, *58*, 29–33.
- (20) Kallen, T. W.; Earley, J. E. *Inorg. Chem.* **1971**, *10*, 1152–1155.
- (21) Adin, A.; Sykes, A. G. *J. Chem. Soc. A* **1966**, 1230–1236.
- (22) Hahn, M.; Wiegardt, K. *Inorg. Chem.* **1984**, *23*, 3977–3982.
- (23) Amadei, G. A.; Earley, J. E. *Croat. Chem. Acta* **2001**, *74*, 601–606.
- (24) Thompson, R. C.; Gordon, G. *Inorg. Chem.* **1966**, *5*, 562–569.
- (25) Thompson, R. C.; Gordon, G. *Inorg. Chem.* **1966**, *5*, 557–562.
- (26) Urbansky, E. T.; Schock, M. R. *J. Environ. Manage.* **1999**, *56*, 79–95.
- (27) Burg, R. V. *J. Appl. Toxicol.* **1995**, *15*, 237–241.
- (28) Schilt, A. A. *Perchloric Acid and Perchlorates*; GFS Chemicals, Inc.: Columbus, OH, 1979.
- (29) Urbansky, E. T. *Biorem. J.* **1998**, *2*, 81–95.
- (30) Logan, B. E. *Biorem. J.* **1998**, *2*, 69–79.
- (31) Herman, D. C.; Frankenberger, W. T. *J. Environ. Qual.* **1999**, *28*, 1018–1024.
- (32) Wallace, W.; Beshear, S.; Williams, D.; Hospadar, S. *J. Ind. Microbiol. Biotechnol.* **1998**, *20*, 126–131.
- (33) Chambliss, C. K.; Odom, M. A.; Martin, C. R.; Moyer, B. A.; Strauss, S. H. *Inorg. Chem. Commun.* **1998**, *1*, 435–438.
- (34) Gu, B.; Brown, G. M.; Maya, L.; Lance, M. J.; Moyer, B. A. *Environ. Sci. Technol.* **2001**, *35*, 3363–3368.

## Scheme 1



proach to developing a practical treatment of perchlorate is the employment of chemical catalysts, since the barrier to perchlorate reduction is kinetic.

As will be shown herein, rhenium complexes featuring the anionic phenoxy-oxazoline or -thiazoline ligand are effective OAT catalysts. These systems present clean reaction chemistry that makes them ideal for quantitative kinetic and mechanistic studies. Fully detailed mechanisms for OAT reactions will be presented on the basis of extensive chemical kinetics, spectroscopic identification of relevant intermediates, substrate variation, electronic effects, and density functional theory (DFT) calculations. The latter has proved in recent years to be a useful tool for addressing mechanistic issues in transition metal chemistry, especially for oxidations and polymerization reactions.<sup>35–43</sup> The reaction kinetics and mechanisms in combination with computational results reveal the factors that control the rate of OAT reactions. The kinetics of oxo transfer from donor substrates to  $\text{Re}^{\text{V}}(\text{O})$  and from  $\text{Re}^{\text{VII}}(\text{O})_2$  to organic acceptors will be contrasted to relevant OAT systems in the literature.

## Results and Discussion

**General Features of Catalysis.** All complexes in Figure 1 were found to catalytically reduce perchlorate to chloride in the presence of organic sulfides under mild conditions (Scheme 1).<sup>16</sup> Under typical steady-state conditions, a 0.8 mol % catalyst loading was employed with  $0.10 \text{ mol L}^{-1}$   $\text{LiClO}_4$  and  $0.50 \text{ M}$  sulfide in  $\text{CH}_3\text{CN}/\text{H}_2\text{O}$  (95:5, v/v) at  $25^\circ\text{C}$ . With catalyst **1** or **2**, the reaction was essentially complete in 2 h irrespective of whether an alkyl or aryl sulfide was used. Steady-state kinetics featured zero-order dependence on sulfide concentration. Since aryl sulfides absorb in the UV range much more intensely than sulfoxides, the kinetics of catalytic perchlorate reduction with thioanisole (PhSMe) were followed at 260 nm. A typical time profile demonstrating zero-order dependence on  $[\text{PhSMe}]$  is shown in Figure 2. Thus, the rate determining step (RDS) involves the reaction of perchlorate and oxorhenium(V). The rise in absorption following the consumption of thioanisole (Figure 2) is due to a change in the steady-state form of the catalyst, that is,

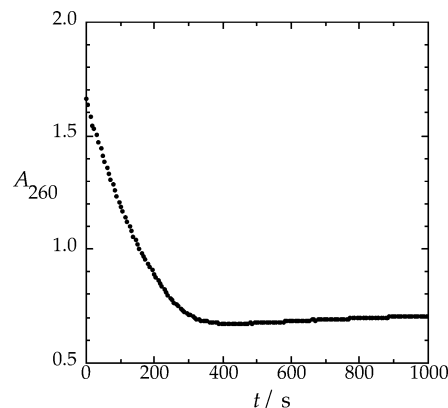


**Figure 2.** Time profile for the oxidation of PhSMe with  $\text{ClO}_4^-$  as catalyzed by complex **2**, monitored at 260 nm (path length = 1.00 mm). Conditions:  $[\text{PhSMe}] = 2.0 \text{ mM}$ ,  $[\text{LiClO}_4] = 0.020 \text{ M}$ , and  $[\mathbf{2}] = 0.20 \text{ mM}$  in  $\text{CH}_3\text{CN}/\text{H}_2\text{O}$  (95:5, v/v) at 293 K.

formation of dioxorhenium(VII), once PhSMe, the limiting reagent, is depleted. The rate of the reaction, however, was retarded by the addition of exogenous chloride due to product inhibition. Qualitatively, chloride inhibition sets in only after 100 turnovers. Chloride inhibits the reaction, since it competes with perchlorate for coordination on rhenium. Both oxazoline rhenium catalysts **1** and **2** exhibited comparable activity, indicating that the two precursor complexes yielded the same active catalytic species. The stoichiometry of the reaction was established on the basis of the yields of isolated sulfoxide under conditions of limiting  $\text{ClO}_4^-$ , and addition of  $\text{AgBF}_4$  at the end of the reaction yielded a quantitative amount of  $\text{AgCl}$ .

The reaction of **1** or **2** with perchlorate as well as with other oxo donors such as  $\text{H}_2\text{O}_2$  and pyridine *N*-oxide (PyO) in the absence of an organic sulfide (or a reductant) revealed the formation of a red-brown intermediate featuring a new absorbance at  $\lambda = 500 \text{ nm}$  ( $\epsilon = 1300 \text{ M}^{-1} \text{ cm}^{-1}$ ). This intermediate has been assigned as the cationic dioxorhenium(VII) complex  $[\text{Re}(\text{O})_2(\text{hoz})_2]^+$ , which forms upon the transfer of an oxygen atom to complex **2**.<sup>16</sup> It is this dioxorhenium(VII) complex that donates an oxo ligand to sulfide, regenerating the starting rhenium(V) catalyst and hence completing the catalytic cycle.

**Mechanism of OAT to Rhenium.** The rate of formation of  $[\text{Re}(\text{O})_2(\text{hoz})_2]^+$  (**4**) from the reaction of **2** with  $\text{ClO}_4^-$  was monitored at 500 nm in 95:5 (v/v)  $\text{CH}_3\text{CN}/\text{H}_2\text{O}$ , under pseudo-first-order conditions, by stopped-flow spectrophotometry. The kinetic measurements revealed a first-order dependence on  $[\mathbf{2}]$  and saturation of the rate at high  $\text{ClO}_4^-$  concentrations (Figure 3). Two kinetically indistinguishable mechanisms would account for the observed saturation in  $[\text{ClO}_4^-]$ . (1) Complex **2** forms an active steady-state intermediate that subsequently reacts with perchlorate (Scheme 2A). (2) Perchlorate reacts with **2** to form, in a prior-equilibrium step, an adduct preceding OAT (Scheme 2B).

The same experiment performed with alternate oxygen donor substrates such as chlorate (Figure 3) and pyridine *N*-oxide (Figure 4) yielded similar kinetic saturation plots but with varying plateau values. Changing the oxo donor in Scheme 2A would have no effect on the saturation value

(35) Torrent, M.; Sola, M.; Frenking, G. *Chem. Rev.* **2000**, *100*, 439–494.

(36) Veldkamp, A.; Frenking, G. *J. Am. Chem. Soc.* **1994**, *116*, 4937–4946.

(37) Deubel, D. V.; Schlecht, S.; Frenking, G. *J. Am. Chem. Soc.* **2001**, *123*, 10085–10093.

(38) Houk, K. N.; Strassner, T. *J. Org. Chem.* **1999**, *64*, 800–802.

(39) Strassner, T.; Busold, M. *J. Org. Chem.* **2001**, *66*, 672–676.

(40) Michalak, A.; Ziegler, T. *Organometallics* **1999**, *18*, 3998–4004.

(41) Deng, L.; Margl, P.; Ziegler, T. *J. Am. Chem. Soc.* **1999**, *121*, 6479–6487.

(42) Chan, M. S. W.; Deng, L.; Ziegler, T. *Organometallics* **2000**, *19*, 2741–2750.

(43) Zeller, A.; Strassner, T. *Organometallics* **2002**, *21*, 4950–4954.

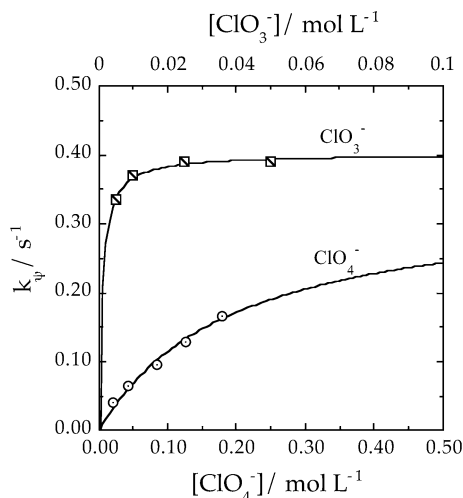
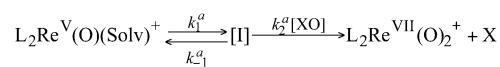


**Figure 3.** Dependence of the observed rate constant ( $k_p$ ) on  $[\text{ClO}_4^-]$  (circles) and  $[\text{ClO}_3^-]$  (hatched squares) for the oxidation of complex **2**.

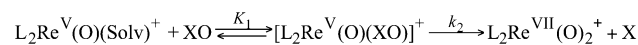
### Scheme 2

A.



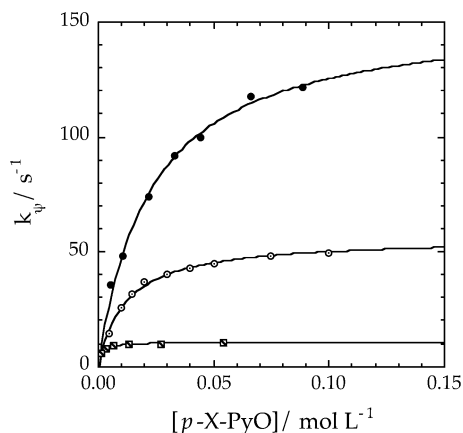
$$\frac{d[\text{L}_2\text{Re}^{\text{VII}}(\text{O})_2^+]}{dt} = \frac{nK_1^a k_2^a [\text{L}_2\text{Re}^{\text{V}}(\text{O})(\text{Solv})^+][\text{XO}]}{1 + k_2^a / k_1^a [\text{XO}]}$$

B.



$$\frac{d[\text{L}_2\text{Re}^{\text{VII}}(\text{O})_2^+]}{dt} = \frac{nK_1 k_2 [\text{L}_2\text{Re}^{\text{V}}(\text{O})(\text{Solv})^+][\text{XO}]}{1 + K_1[\text{XO}]}$$

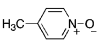
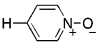
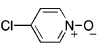
L = hoz; Solv = solvent ( $\text{H}_2\text{O}$  or  $\text{CH}_3\text{CN}$ ); XO =  $\text{ClO}_4^-$ ,  $\text{ClO}_3^-$ , or PyO; and  $n$  = stoichiometric coefficient:  $n = 4$  for  $\text{ClO}_4^-$ ,  $n = 3$  for  $\text{ClO}_3^-$ , and  $n = 1$  for PyO.



**Figure 4.** Dependence of the observed rate constant ( $k_p$ ) for the oxidation of complex **2** on the pyridine *N*-oxide substrates: *p*-Me-PyO (hatched squares), PyO (open circles), and *p*-Cl-PyO (closed circles).

( $k_1^a$ ), which is not consistent with experimental observations. However, in Scheme 2B, the saturation value is governed by  $k_2$ , which would change according to the identity of the oxidant bound to the metal. In conclusion, Scheme 2B and its rate law satisfy the observed experimental results. The equilibrium constants ( $K_1$ 's) and rate constants ( $k_2$ 's) for OAT to complex **2** from several donor substrates are summarized in Table 1. While the rate measurements reported for the

**Table 1.** Kinetics Data for OAT to Complex **2**<sup>a</sup>

Oxo donor (XO)	$K_1/\text{M}^{-1}$	$k_2/\text{s}^{-1}$	$K_1 k_2/\text{M}^{-1} \text{s}^{-1}$	$\Delta G^\circ_{\text{XO/X}} (\text{XO} = \text{X} + 1/2\text{O}_2)/\text{kJ mol}^{-1}$
$\text{ClO}_4^-$	$5 \pm 1$	$0.09 \pm 0.01$	0.45	0.59 <sup>b</sup>
$\text{ClO}_3^-$	$208 \pm 26$	$0.134 \pm 0.002$	28	25.1 <sup>b</sup>
	$714 \pm 60$	$11 \pm 1$	7,854	—
	$83 \pm 5$	$56 \pm 1$	4,648	33 <sup>c</sup>
	$44 \pm 5$	$154 \pm 6$	6,776	—
t-BuOOH	$2.0 \pm 0.4$	$80 \pm 10$	160	-42 <sup>d</sup>

<sup>a</sup> The reactions with  $\text{ClO}_4^-$  and  $\text{ClO}_3^-$  were carried out in 95:5 (v/v)  $\text{CH}_3\text{CN}/\text{H}_2\text{O}$  at 293 K, and the reactions with PyO substrates and t-BuOOH were done in  $\text{CH}_3\text{CN}$  at 293 K. <sup>b</sup> The thermodynamic data for perchlorate and chlorate reduction to chlorate and chlorite, respectively, measured in an acidic aqueous medium are from ref 44. <sup>c</sup> Estimated from the enthalpy change for PyO to Py in the gas phase, ref 45, assuming  $\Delta S_{\text{XO/X}} = 66 \text{ J mol}^{-1} \text{ K}^{-1}$ . <sup>d</sup> The thermodynamic data for t-BOOH to BuOH in the liquid phase are from ref 44.

**Table 2.** Calculated Free Energies for the Stepwise Reduction of  $\text{ClO}_4^-$  to  $\text{Cl}^-$

reaction <sup>a</sup>	$\Delta G^\circ/\text{kJ mol}^{-1}$
$\text{ClO}_4^- + \text{Re}(\text{O})\text{L}_2^+ \rightarrow \text{ClO}_3^- + \text{Re}(\text{O})_2\text{L}_2^+$	-69.5
$\text{ClO}_3^- + \text{Re}(\text{O})\text{L}_2^+ \rightarrow \text{ClO}_2^- + \text{Re}(\text{O})_2\text{L}_2^+$	-39.2
$\text{ClO}_2^- + \text{Re}(\text{O})\text{L}_2^+ \rightarrow \text{ClO}^- + \text{Re}(\text{O})_2\text{L}_2^+$	-134.7
$\text{ClO}^- + \text{Re}(\text{O})\text{L}_2^+ \rightarrow \text{Cl}^- + \text{Re}(\text{O})_2\text{L}_2^+$	-232.3
sum: $[\text{ClO}_4^- + 4\text{Re}(\text{O})\text{L}_2^+ \rightarrow \text{Cl}^- + 4\text{Re}(\text{O})_2\text{L}_2^+]$	-475.7

<sup>a</sup> L = hoz = 2-(2'-hydroxyphenyl)-2-oxazoline.

PyO substrates and t-BuOOH were performed in acetonitrile instead of the mixed solvent system (95:5  $\text{CH}_3\text{CN}/\text{H}_2\text{O}$ ) used with perchlorate and chlorate, the kinetics of  $[\text{Re}(\text{O})_2(\text{hoz})_2]^+$  formation were found to be independent of water concentration up to 5.3 M (9.5 vol %).

It is noteworthy that while rate saturation sets in at high concentrations (0.10 M) for  $\text{ClO}_4^-$ , it is clearly evident at low concentrations (0.0050 M) for  $\text{ClO}_3^-$  (Figure 3) and for the pyridine *N*-oxide substrates (Figure 4). The rate of OAT ( $k_2$ ) for PyO is more than 2 orders of magnitude faster than the value observed for  $\text{ClO}_4^-$ , despite the lower driving force (Table 1). The reduction of perchlorate to chloride by complex **2** is an exergonic process. Calculated Gibbs free energies (by DFT) for successive oxo transfers from perchlorate to oxorhenium(V) are given in Table 2. On the basis of the known  $\Delta G^\circ_{\text{XO/X}}$  values for perchlorate and chlorate reduction by OAT (Table 1) and our calculated values for OAT from these two oxyanions to complex **2** (Table 2), an average  $\Delta G^\circ$  value for the reaction  $(\text{hoz})_2\text{Re}^{\text{V}}(\text{O})^+ + 1/2\text{O}_2 \rightarrow (\text{hoz})_2\text{Re}^{\text{VII}}(\text{O})_2^+$  of  $-67 \pm 3 \text{ kJ mol}^{-1}$  can be determined (see the Supporting Information for the thermodynamic calculation). This value is in reasonable agreement with an upper limit of  $-84 \text{ kJ mol}^{-1}$  that was set by means of a thermodynamic cycle for the couple  $\text{Re}^{\text{V}}(\text{O})/\text{Re}^{\text{VII}}(\text{O})_2$ .<sup>46</sup>

(44) Lide, D. R., Ed. *The NBS Tables of Chemical Thermodynamic Properties*; American Chemical Society and American Institute for Physics: Washington, DC, 1982, Vol. 11, supplement no. 2.

(45) Li, S.; Pilcher, G. J. *Chem. Thermodyn.* **1988**, *20*, 463.

(46) Arias, J.; Newlands, C. R.; Abu-Omar, M. M. *Inorg. Chem.* **2001**, *40*, 2185-2192.

**Table 3.** Activation Parameters for OAT Reactions ( $k_2$ 's) from  $\text{ClO}_3^-$  and  $p\text{-CH}_3\text{-PyO}$  to Complex **2**<sup>a</sup>

	$\text{ClO}_3^-$	$p\text{-CH}_3\text{-PyO}$
$\Delta H^\ddagger/\text{kJ mol}^{-1}$	$54 \pm 1$	$66 \pm 2$
$\Delta S^\ddagger/\text{J mol}^{-1} \text{K}^{-1}$	$-28 \pm 3$	$0 \pm 5$
$E_a/\text{kJ mol}^{-1}$	$57 \pm 1$	$68 \pm 2$
$A (\times 10^{11})/\text{s}^{-1}$	$6 \pm 2$	$167 \pm 100$

<sup>a</sup> Experimental conditions:  $[\mathbf{2}] = 5.0 \times 10^{-4} \text{ M}$ ,  $[p\text{-CH}_3\text{-PyO}] = 0.109 \text{ M}$ ,  $[\text{ClO}_3^-] = 6.76 \text{ mM}$ ,  $\lambda_{\text{obs}} = 500 \text{ nm}$ .

The discrepancy between kinetics and thermodynamics is a recurring theme in metal mediated OAT reactions, and the systems presented here are no exception.<sup>9,10,47</sup> Factors other than thermodynamics dictate the rate of atom transfer. Chlorate reacts faster with complex **2** not because it is a better oxo donor than perchlorate but rather because it is a better ligand (Table 1). Note that the values of  $k_2$  for both oxyanions are comparable, despite the fact that perchlorate is the better oxidant of the two; however, the values of  $K_1$  differ significantly.

One of the most attractive features of the reaction kinetics of our rhenium oxazoline system is the separation of the oxo donor coordination step from the atom transfer event. For most systems, the kinetics are first-order in the transition metal complex and in the oxo donor substrate, and as a result, the kinetic information is a composite of ligand substitution (oxo donor coordination to the metal center) and oxo transfer.<sup>9,10,47</sup> Furthermore, examples have been noted in the literature in which ligand substitution is rate determining.<sup>8</sup> Therefore, complex **2** presented an excellent opportunity to investigate factors that affect the rate of OAT reactions. To understand these factors, we investigated the kinetics of OAT to complex **2**, employing pyridine *N*-oxide substrates with different substituents in the para position (Figure 4 and Table 1). As evident by the values of  $K_1$  and  $k_2$  for the different PyO substrates, an electron-donating substituent makes the PyO substrate a better ligand but an inferior oxygen donor. Therefore, from a structure–reactivity standpoint, the transition state for OAT ( $k_2$ ) features a negative charge buildup on the PyO nitrogen as the N–O bond weakens and the Re=O bond is formed, which is also supported by DFT calculations (vide infra). It is noteworthy that, without the separation of rate constants, the second-order rate constant ( $K_1k_2$ ) (Table 1) would not have provided a method for probing the electronic effects on oxygen atom transfer, as both electron-donating and electron-withdrawing substituents appear to enhance the reaction rate.

The temperature dependence of OAT ( $k_2$ ) was determined for  $\text{ClO}_3^-$  and  $p\text{-CH}_3\text{-PyO}$  in the limit of substrate saturation (Table 3). The activation parameters for  $k_2$  were determined using a least-squares fitting to the transition state theory expression, eq 4. The enthalpy of activation values for both  $\text{ClO}_3^-$  and  $p\text{-CH}_3\text{-PyO}$  are comparable (Table 3), and they are consistent with what has been measured for other OAT systems.<sup>8,10,47–49</sup> The entropy of activation values are, on the other hand, different for the two oxo donors. Oxygen atom

transfer from  $p\text{-CH}_3\text{-PyO}$  has a  $\Delta S^\ddagger$  value of zero, indicating a monomolecular oxygen transfer reaction (i.e., no entropy change from the precursor complex  $[\text{Re}^{\text{V}}\text{-OX}]$  to the transition state). This is in agreement with theoretical calculations which show no loss of translational or rotational entropy going from the adduct  $[\text{Re}^{\text{V}}\text{-OX}]$  to the transition state. The  $\Delta S^\ddagger$  value for  $\text{ClO}_3^-$ , however, is negative but much smaller than that previously observed for OAT reactions of rhenium and molybdenum complexes.<sup>8,10,47–49</sup> Typical values of  $\Delta S^\ddagger$  for oxo transfer from substrates to metal complexes have been noted in the range  $-80$  to  $-140 \text{ J mol}^{-1} \text{K}^{-1}$ . The source of the difference in  $\Delta S^\ddagger$  for  $\text{ClO}_3^-$  and  $p\text{-CH}_3\text{-PyO}$  is not fully understood, except that the transition state for  $\text{ClO}_3^-$  must involve more geometrical changes from the structure of the precursor  $\text{ClO}_3^-$  adduct than in the case of  $p\text{-CH}_3\text{-PyO}$ .

$$k = \frac{k_{\text{B}}T}{h} e^{(\Delta S^\ddagger/R)} e^{(-\Delta H^\ddagger/RT)} \quad (4)$$

In summary, OAT from substrates proceeds via the formation of a precursor adduct,  $[\text{Re}^{\text{V}}\text{-OX}]$ , which is supported by saturation kinetics. The atom transfer step is very sensitive to electronic changes on the substrate. Electron-withdrawing substituents enhance the rate of oxo transfer ( $k_2$ ), demonstrating a negative charge buildup on the substrate in the transition state. The bulk of the activation barrier to oxo transfer is enthalpic, and in the case of PyO,  $\Delta S^\ddagger$  is zero. The factors that control the rate of OAT thus are (1) facile precursor adduct formation, (2) the absence of an entropic change as the complex  $[\text{Re}^{\text{V}}\text{-OX}]$  proceeds to the transition state structure, and (3) the minimization of the reorganization energy required to make products from the precursor complex.

**Dynamic Behavior of **2** and **2a** and Its Relevance to  $[\text{Re}^{\text{V}}\text{-OX}]$  Adduct Formation.** The most significant structural change along the oxygen atom transfer reaction pathway takes place during the formation of the adduct  $[\text{Re}^{\text{V}}\text{-OX}]$ . The rhenium catalyst begins with the solvent ligand ( $\text{H}_2\text{O}$  or  $\text{CH}_3\text{CN}$ ) in a trans configuration with respect to  $\text{Re}=\text{O}$  and the oxazoline ligands occupying the equatorial plane (Scheme 3). In the OAT product,  $(\text{hoz})_2\text{Re}^{\text{VII}}\text{O}_2^+$ , the two oxo ligands are arranged cis to each other, as would be expected for a  $d^0$  metal center. Therefore, the oxo donor substrate (such as  $\text{ClO}_4^-$  and PyO) can be expected to either coordinate trans followed by a subsequent rearrangement to cis or enter cis to the oxo ligand initially (Scheme 3). Either mechanism could occur associatively or dissociatively. The earlier mechanism is accomplished via a rotation about a pseudo- $C_3$  axis of the octahedron comprising an oxazoline (hoz) ligand and the oxo donor substrate (XO). This is termed a turnstile mechanism and has been suggested for dithiolate rhenium(V) compounds.<sup>50</sup> In the second mechanism, XO enters into the equatorial plane, forming a pentagonal

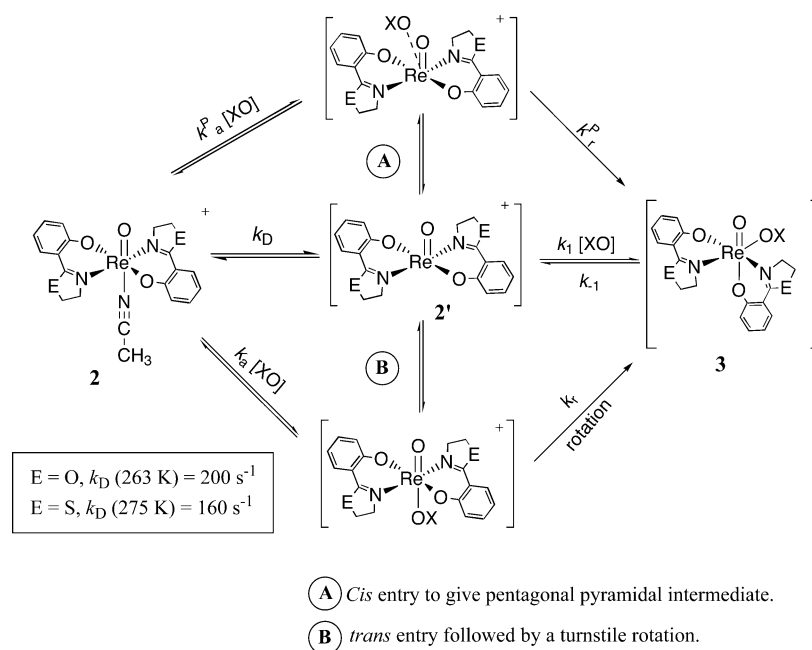
(48) Topich, J.; Lyon, J. T., III. *Inorg. Chem.* **1984**, *23*, 3202–3206.

(49) Roberts, S. A.; Young, C. G.; Cleland, W. E., Jr.; Ortega, R. B.; Enemark, J. H. *Inorg. Chem.* **1988**, *27*, 3044–3051.

(50) Lahti, D. W.; Espenson, J. H. *J. Am. Chem. Soc.* **2001**, *123*, 6014–6024.

(47) Abu-Omar, M. M.; Appelman, E. H.; Espenson, J. H. *Inorg. Chem.* **1996**, *35*, 7751–7757.

Scheme 3



pyramidal structure; subsequent or concurrent to that, the phenoxide of the hoz ligand moves to assume the coordination position *trans* to the oxo ligand. The *cis* entry of XO is favored on the basis of DFT calculations (*vide infra*).

Variable temperature (VT)  $^1\text{H}$  NMR studies of complexes **2** and **2a** in  $\text{CD}_3\text{CN}$  revealed a temperature dependence on the oxazoline ligand proton signals (Figure 5). Each peak splits into two separate peaks, each retaining their original multiplicity. Neither set of peaks corresponded with the free oxazoline ligand  $^1\text{H}$  spectrum, indicating that the ligand was not dissociating. A lack of signal change in VT  $^{19}\text{F}$  NMR ruled out triflate substitution. Addition of 0.010–1.0 M  $\text{H}_2\text{O}$  to the solution had no effect on the coalescence temperature and therefore excluded  $\text{H}_2\text{O}$  from the equilibrium. Since both sets of peaks still resemble the original spectrum pattern of **2** with a  $C_2$  axis (that is two equivalent hoz ligands), the observed temperature dependence can only be attributed to a dynamic equilibrium of **2** with a five-coordinate species in which acetonitrile leaves to create an open coordination site *trans* to the oxo ligand, retaining the complex's  $C_2$  axis (Scheme 3).

The coalescence temperature for the oxazoline complex **2** in  $\text{CD}_3\text{CN}$  is 263 K, and the first-order rate constant ( $k_D$ ) at the coalescence temperature according to the approximate relationship in eq 5 is  $200 \text{ s}^{-1}$ . The thiazoline complex **2a** exhibits similar behavior and has a coalescence temperature of 275 K and a  $k_D$  value of  $160 \text{ s}^{-1}$ . The rapid kinetics associated with this dynamic process facilitates the geometrical changes necessary for the formation of the adduct [*cis*- $\text{L}_2\text{Re}^{\text{V}}(\text{O})(\text{OX})$ ] (**3**) responsible for effective oxygen atom transfer to rhenium. The kinetic constants ( $k_D$ 's) show that the thiazoline complex **2a** is less fluxional than its oxazoline analogue, yet the  $k_D$  value for **2a** is still faster than the rate determining step of OAT. In summary, it is desirable to have a stable but fluxional ligand system that can accommodate with ease the necessary geometrical changes

for binding oxo donor substrates. It is noteworthy that once the dioxorhenium(VII) complex **4** is formed in the specified stereochemistry (all-*cis*, see below), it does not isomerize to **4''** (*trans*- $\text{N}_{\text{hoz}}$ ), as the oxazoline ligand is tightly bound and does not undergo a change from bidentate to monodentate readily. Thus, the facile ligand rearrangement is achieved via the availability of a labile solvent molecule in the rhenium coordination sphere (Scheme 3) and not by a dissociative oxazoline ligand that interchanges between bidentate and monodentate.

$$k \cong \frac{\pi(\delta\nu)}{\sqrt{2}} \quad (5)$$

**OAT from Dioxorhenium(VII).** The red dioxorhenium(VII) complex **4** can be prepared in situ by the stoichiometric reaction of **2** with  $\text{PyO}$ .<sup>16</sup> Even though **4** decomposes with water (*vide infra*), it persists for weeks in dry acetonitrile. Therefore, its reactions with organic thioethers and other substrates were investigated under pseudo-first-order conditions by stopped-flow spectrophotometry. The progress of the reaction was monitored at 500 nm, where complex **4** absorbs but not complex **2**. Another method of following oxo transfer to a substrate from **4** that verifies the integrity of complex **4** is to employ sequential mixing on the stopped-flow. A stoichiometric amount of  $\text{PyO}$  and **2** were mixed to allow for complete formation of dioxorhenium(VII) followed by the addition of excess sulfide after a programmed time delay. In this second method, the formation of **4** was followed to completion, and freshly formed **4** was reacted immediately with a substrate. The values from both methods were consistent. The second-order rate constants ( $k_3$ 's) for the reactions of **4** with the thioether substrates are given in Table 4. The rate constants of OAT to a substrate amazingly span 7 orders of magnitude over a range of  $\sim 200 \text{ kJ mol}^{-1}$  in the  $\Delta G$  value of the reaction.

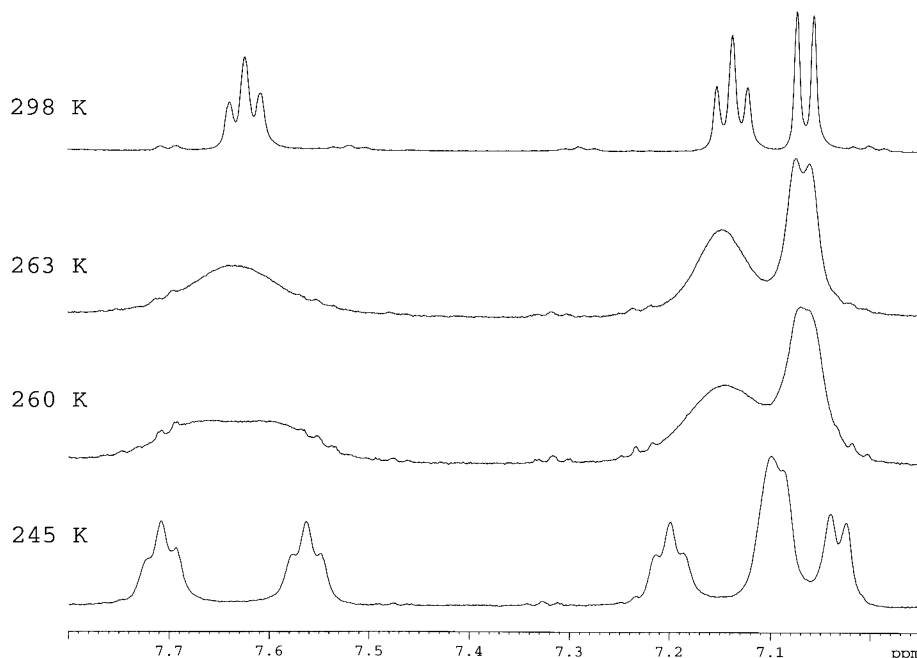


**Figure 5.** Variable temperature  $^1\text{H}$  spectra of complex **2** in  $\text{CD}_3\text{CN}$  showing the aromatic region.

**Table 4.** Second-Order Rate Constants for the Following Oxo Transfer Reaction:  $(\text{hoz})_2\text{Re}(\text{O})_2^+ + \text{Y} \rightarrow (\text{hoz})_2\text{Re}(\text{O})^+ + \text{YO}^a$

substrate (Y)	$k_3$ (293 K)/ $\text{L mol}^{-1} \text{s}^{-1}$	$\Delta G^\circ_{\text{Y/YO}} (\text{Y} + 1/2\text{O}_2 = \text{YO})/\text{kJ mol}^{-1}$
$\text{H}_3\text{CSCCH}_3$	$7500 \pm 300$	$-88.6^b$
$\text{H}_3\text{CS}(\text{O})\text{CH}_3$	$0.85 \pm 0.05$	$-191.2^b$
$\text{CH}_3\text{CH}_2\text{SCH}_2\text{CH}_3$	$6900 \pm 200$	
$(\text{CH}_3)_3\text{CSC}(\text{CH}_3)_3$	$1482 \pm 79$	
$(p\text{-OCH}_3\text{-C}_6\text{H}_4)\text{SCH}_3$	$1271 \pm 100$	
$(p\text{-CH}_3\text{-C}_6\text{H}_4)\text{SCH}_3$	$367 \pm 25$	
$(\text{C}_6\text{H}_5)\text{SCH}_3$	$110 \pm 8$	$-94^c$
$(p\text{-Cl-C}_6\text{H}_4)\text{SCH}_3$	$2.6 \pm 0.2$	
$(p\text{-CN-C}_6\text{H}_4)\text{SCH}_3$	$0.091 \pm 0.005$	
$(\text{C}_6\text{H}_5)_2\text{S}(\text{C}_6\text{H}_5)$	$1.1 \pm 0.1$	$-100^c$
$(\text{C}_6\text{H}_5)_3\text{P}$	$> 10^6$	$-284^c$

<sup>a</sup> The reactions were carried out on a stopped-flow analyzer under pseudo-first-order conditions in acetonitrile at 25 °C with **[4]** = 0.50 mM (prepared in situ from **2** and equimolar 4- $\text{CH}_3$ -PyO) and **[Y]** = 4.0–90.0 mM. <sup>b</sup> From ref 44. <sup>c</sup> Estimated from  $\Delta H_{\text{Y/YO}}$ , refs 1 and 51, on the basis of a value for  $\Delta S_{\text{Y/YO}}$  similar to that for MeSMe ( $-83 \text{ J mol}^{-1} \text{ K}^{-1}$ ).

The general trend of the rate constants ( $k_3$ 's) is indicative of electrophilic oxo transfer from **4** to the substrate. Aryl sulfides are less reactive than alkyl sulfides, and sulfides are much more reactive than the corresponding sulfoxides, which explains the high product selectivity for sulfoxide. Furthermore, only a lower limit can be put on the reaction of **4** with  $\text{PPh}_3$ , since the reaction is faster than the stopped-flow dead time. To probe the electronic sensitivity of OAT from complex **4**, we determined the rate constants for a few phenylmethyl sulfide derivatives containing substituents in the para position (Table 4). The structure–reactivity correlation of Hammett was employed to gain insight into the nature of the transition state.<sup>52</sup> The Hammett plot of  $\log(k_3^{\text{H}}/k_3^{\text{X}})$  versus  $\sigma_p$  yielded a reaction constant of  $\rho = -4.6 \pm 0.4$  ( $R = 0.991$ ). The negative sign of the reaction constant indicates a positive charge buildup on the sulfur in the transition state and shows it is in agreement with nucleophilic attack of a substrate on an electrophilic oxo ligand.

It is noteworthy that the second-order rate constants ( $k_3$ 's) for sulfides are larger than the  $K_1k_2$  value (apparent second-order rate constant, Scheme 2) for perchlorate reduction. Therefore, under steady-state (catalytic) conditions, the formation of the dioxorhenium(VII) complex **4** is rate determining and the dominant form of the catalyst is rhenium(V).

#### Properties of the Cationic Dioxorhenium(VII) Complex

**4.** In the absence of an oxygen atom acceptor (sulfide), the red dioxorhenium(VII) complex **4** hydrolyzes to  $(\text{hoz})\text{Re}(\text{O})_3$  (**5**) with first-order dependence on  $[\text{Re}]$  and  $[\text{H}_2\text{O}]$  ( $k_4$  (293 K) =  $(2.8 \pm 0.2) \times 10^{-4} \text{ L mol}^{-1} \text{ s}^{-1}$ ). Interestingly, the resulting neutral trioxorhenium(VII) is not active in OAT reactions. It reacts neither with sulfides nor with organic phosphines. For example,  $\text{PPh}_3$  coordinates to **5** ( $^{31}\text{P}$  NMR:  $\delta -3.7$ ) instead of being oxidized to  $\text{O}=\text{PPh}_3$ . The three  $\pi$ -donating oxo ligands stabilize the +7 oxidation state. In comparison,  $\text{PPh}_3$  reduces  $(\text{hoz})_2\text{Re}(\text{O})_2^+$  with a second-order rate constant that is  $> 10^6 \text{ L mol}^{-1} \text{ s}^{-1}$ . However, under dry conditions, **4** persists for days in acetonitrile or dichloromethane and has been fully characterized by mass spectrometry and  $^1\text{H}$  NMR.<sup>16</sup> Crystallization of **4** (with chloride anion) in the drybox yielded single crystals after 4–7 days of a neutral amidato complex, **6** (Figure 6), which contains a ring-opened oxazoline ligand in accordance to the transformation in eq 6. The  $\text{Re}-\text{N}(2)$  (anionic amidato ligand) distance is 2.018(3) Å versus a  $\text{Re}-\text{N}(1)$  (neutral oxazoline ligand) distance of 2.272(3) Å. The  $\text{C}(16)-\text{O}(6)$  distance of the amidato ring-opened ligand is 1.235(4) Å, which is consistent with a  $\text{C}=\text{O}$  double bond. However, some electron delocalization with the amidato nitrogen is evident in the structural data, as the  $\text{C}(16)-\text{N}(2)$  distance is 1.380(5) Å

(51) Jenks, W. S.; Matsunaga, N.; Gordon, M. *J. Org. Chem.* **1996**, *61*, 1275–1283 and references therein.

(52) Hammett, L. P. *Physical Organic Chemistry*; McGraw-Hill Book Co.: New York, 1940.

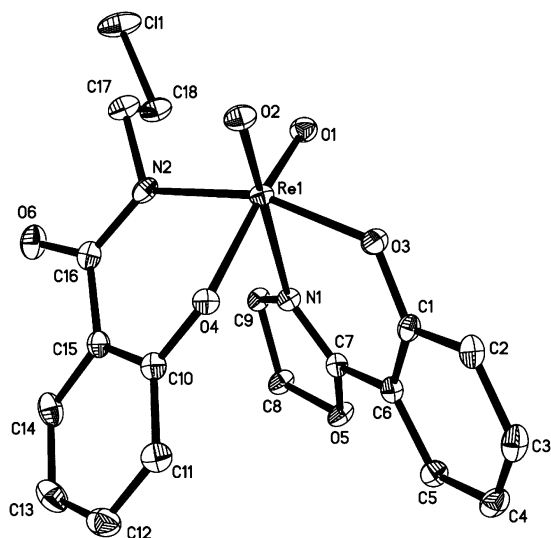
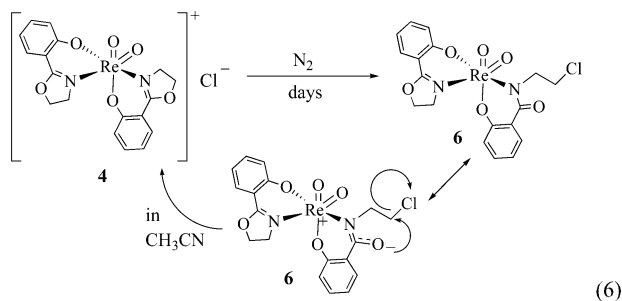


**Figure 6.** Structure of the dioxorhenium(VII) complex **6** showing the 50% probability ellipsoids and the atom labeling scheme. Hydrogen atoms are not included for clarity. Selected bond lengths (angstroms) and angles (deg): Re–O1 = 1.717(3), Re–O2 = 1.712(3), Re–O3 = 1.917(2), Re–O4 = 1.970(2), Re–N1 = 2.272(3), Re–N2 = 2.018(3), C16–O6 = 1.235(4), C16–N2 = 1.380(5), C17–N2 = 1.490(4), C18–C11 = 1.794(4), C7–N1 = 1.286(4), C9–N1 = 1.485(4), C7–O5 = 1.332(4), C8–O5 = 1.470(4), O1–Re–O2 = 102.36(13), O4–Re–N2 = 83.17(11), C17–N2–C16 = 113.8(3), O6–C16–N2 = 120.5(3), C1–C18–C17 = 109.5(3), C9–N1–C7 = 107.3(3), N1–C7–O5 = 117.3(3), and C7–O5–C8 = 106.3(3).

versus a C(17)–N(2) distance of 1.490(4) Å. The latter distance is typical for a C–N single bond, yet the former distance (C(16)–N(2)) is between that of a single bond and that of a double bond, similar to the C–N distances observed in aromatic rings. We also observe similar delocalization in the oxazoline ring ligands; for example, the C(7)–O(5) distance is 1.332(4) Å versus a C(8)–O(5) distance of 1.470(4) Å. The C(18)–C1 distance is 1.794(4) Å, which is in the expected range for a C–Cl single bond.



To better understand the role of **6** in catalytic oxo transfer from perchlorate, we decided to measure the kinetics of OAT reactions from **6** to organic thioethers. Upon dissolution of crystalline **6** into acetonitrile, it reverted to the cationic dioxorhenium(VII) complex **4**. Even though puzzling at the offset, this observation can be understood once the synthesis of the oxazoline ligand is carefully considered. Following the reaction of ethyl salicylate with amino alcohol, the amide product is treated with thionyl chloride to replace the alkyl OH group with a better leaving group, namely, Cl. The oxazoline ring is then closed upon treatment with a mild base. Therefore, the amidato ligand in complex **6** is activated

for ring closure by the Lewis acidic rhenium(VII) center (eq 6). The molecular structure of **6** provides support for the proposed mechanism. The X-ray data shows delocalization of the carbonyl double bond with the adjacent C–N bond, as discussed above. Calculations confirm electron delocalization, as can be seen from Figure 7. The amidato oxygen carries a significant negative charge (−0.47). Also, the oxygens of the oxazoline ligands in both complexes **4** and **6** feature Mulliken charges (−0.44 to −0.47) that are comparable to those displayed by the nitrogens of oxazoline (−0.48 to −0.67). Natural bond orbital/natural population analysis (NBO/NPA) calculations have also yielded a similar charge distribution with very subtle variations from the Mulliken charges (see the Supporting Information).

In summary, the ring-opened amidato product is not a step toward catalyst deactivation, since it takes place over a period of days and the resulting complex, **6**, repairs itself by reverting back to the active form of the catalyst, complex **4**. However, the mechanism of ring-opening by chloride could potentially be accomplished by any other nucleophile, such as OH<sup>−</sup> or H<sub>2</sub>O. The hydrolytic deactivation of complex **4** could proceed initially with such a mechanism. However, the latter pathway to give (hoz)ReO<sub>3</sub> (**5**) is insignificant under steady-state conditions because the catalyst is present predominantly (>99%) in the rhenium(V) form, which is stable indefinitely, and the rate of OAT to sulfides is much faster than that of deactivation by water. In fact, the only noticeable deceleration of the catalyst's activity is due to product (Cl<sup>−</sup>) inhibition. Once chloride is removed by precipitation with AgBF<sub>4</sub>, the catalyst regains full activity in successive cycles without any sign of catalyst loss even after hundreds of turnovers.

**Effects of Sulfur versus Oxygen in the Second Coordination Sphere.** Metalloenzymes utilize noncovalent interactions and the second coordination sphere in their active sites to control substrate binding as well as to tune substrate activation and accessibility of the transition state.<sup>53,54</sup> A thiazoline analogue of oxazoline (Figure 1) was investigated in the context of oxo transfer reactions because it allows direct comparisons between oxygen and sulfur in the second coordination sphere of rhenium. Both thiazoline complexes **1a** and **2a** were successfully synthesized and fully characterized (by <sup>1</sup>H NMR, mass spectrometry (MS), X-ray, and elemental analysis). The phenoxy-thiazoline ligand chelates rhenium through the anionic phenoxide oxygen and the neutral thiazoline nitrogen. The sulfur of thiazoline does not bind to rhenium. Figure 8 displays an ORTEP of the molecular structure of complex **1a**. Complex **2a**, which is green in color, reacts with perchlorate to give a red dioxorhenium(VII) complex, **4a**, similar to that observed for the oxazoline complex. The rate constant for the reaction of **2a** with ClO<sub>4</sub><sup>−</sup> is less than that measured for **2** by a factor of 2. Furthermore, the kinetics of the reaction of **2a** with PyO is comparable to that observed for the parent oxazoline complex **2** (Table 5). Hence, the rate of oxo transfer from a substrate to rhenium is not influenced significantly by varying

(53) Lipscomb, W. N.; Strater, N. *Chem. Rev.* **1996**, *96*, 2375–2434.

(54) Lu, Y.; Valentine, J. S. *Curr. Opin. Struct. Biol.* **1997**, *7*, 495–500.



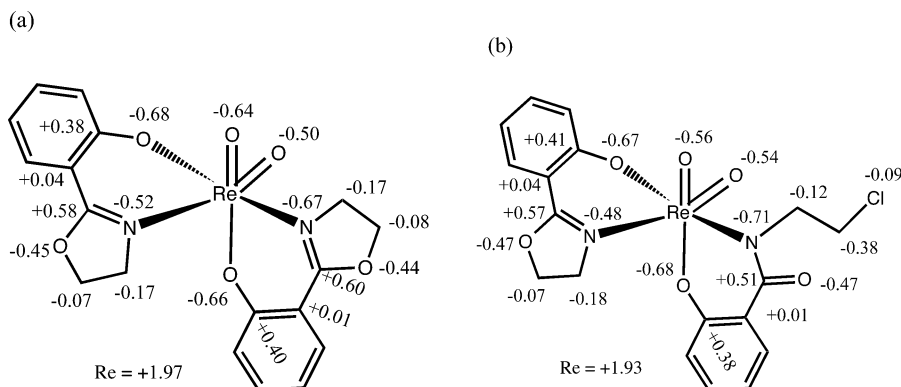


**Figure 7.** Charge distribution of the (a) cationic dioxorhenium(VII) complex **4** and (b) neutral dioxorhenium(VII) complex **6**. Only relevant atoms are shown with their Mulliken charges.

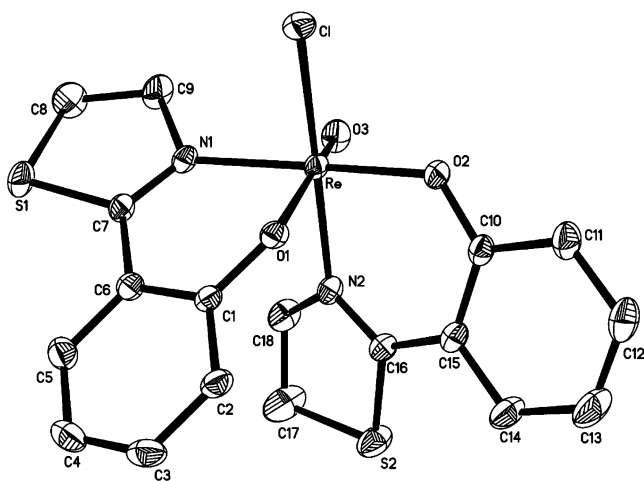
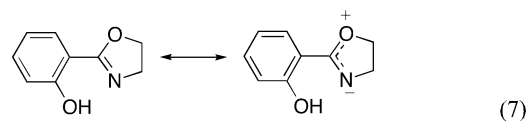


**Figure 8.** Structure of the rhenium(V) thiazoline complex **1a** showing the 50% probability ellipsoids and the atom labeling scheme. Selected bond lengths (angstroms) and angles (deg): Re–O3 = 1.688(3), Re–Cl = 2.3669(11), Re–O1 = 1.997(3), Re–O2 = 1.983(3), Re–N1 = 2.111(3), Re–N2 = 2.103(4), C7–N1 = 1.298(5), C9–N1 = 1.474(5), C7–S1 = 1.743(4), C8–S1 = 1.795(6), C16–N2 = 1.294(5), C18–N2 = 1.470(5), C16–S2 = 1.754(4), C17–S2 = 1.798(7), O1–Re–O3 = 165.13(15), Cl–Re–O3 = 102.62(13), N1–Re–O2 = 166.10(13), C1–O1–Re = 127.4(2), and C7–N1–Re = 127.6(3).

O to S in the heterocyclic ligand moiety; the reaction proceeds slightly slower with thiazoline than with oxazoline. However, when the kinetics of OAT from the dioxorhenium(VII) complexes **4** and **4a** were compared, the rate of oxo transfer from the thiazoline complex **4a** was found to be 18 times faster than that measured for its oxazoline counterpart, complex **4** (Table 5). This difference is much larger than the factor of 2 observed for oxo transfer from a substrate. Furthermore,  $(\text{thoz})_2\text{Re}^{\text{VII}}(\text{O})_2^+$  (**4a**) is less stable than complex **4** and is more susceptible to hydrolytic degradation (Table 5).

The differences in reactivity and stability between the dioxorhenium(VII) oxazoline and thiazoline complexes can be reconciled by considering the size differences between sulfur and oxygen as well as the extent of  $\pi$ -electron delocalization in the respective ring structures. Since sulfur has larger and more diffused p-orbitals than oxygen, its ability to  $\pi$ -conjugate with the C=N double bond in the heterocyclic ligand is less than that of oxygen in oxazoline (eq 7). This rationalization is supported by structural data on oxazoline and thiazoline complexes. The X-ray molecular

structure of complex **1a** (Figure 8) shows no delocalization of the C=N  $\pi$ -electrons with sulfur, C(7)–S(1) = 1.743(4) Å and C(8)–S(1) = 1.795(6) Å. In contrast, the structures of the rhenium(V) oxazoline complexes as well as the dioxorhenium(VII) complex **6** display significant delocalization of the  $\pi$ -electrons with oxygen (Table 6). The distance between oxygen and the  $\text{sp}^2$  carbon (the 2 position) in the oxazoline ring is in the range 1.32–1.36 Å, which is significantly shorter than a C–O single bond and shorter than the C( $\text{sp}^3$ )–O distance (1.45–1.48 Å) in the oxazoline ring. Table 6 summarizes and contrasts selected bond lengths that demonstrate this difference in  $\pi$ -delocalization between oxazoline and thiazoline for complexes **1a**, **2**, and **6**. Therefore, per the resonance contribution shown in eq 7, the oxazoline ligand stabilizes the higher oxidation state of rhenium (+7) more effectively than thiazoline.



The resonance contribution can also be found in the atomic charges for anionic hoz (Figure 9a) and its sulfur analogue thoz (Figure 9b). Their Mulliken charges are given for the anionic ligands. The five-membered rings show a significantly different charge distribution. Due to the higher electronegativity, the hoz-O2 carries a bigger negative charge than the thoz-S1. This corresponds to a greater delocalization of  $\pi$ -electrons from N1 via C1 to O2, while the thoz ligand shows no charge at S1 or C1 but partially negative charges on N1 and C2.

The possibility that the lack of stability of  $(\text{thoz})_2\text{Re}^{\text{VII}}(\text{O})_2^+$  (**4a**) was originating from ligand oxidation at sulfur was explored. No evidence of ligand oxidation was found. Addition of an exogenous free ligand (Hthoz) did not affect the kinetics of decomposition, and no oxidized ligand (Hthoz–SO) was recovered. Furthermore, the kinetics of decomposition of complex **4a** is first-order and not second-order in rhenium.

Since the RDS in perchlorate reduction is the OAT from  $\text{ClO}_4^-$  to rhenium(V), the thiazoline complex **2a** is not a better catalyst than its oxazoline analogue, complex **2**, despite its enhanced rate of reaction with sulfides. On the contrary,

**Table 5.** Comparison of the Kinetic Constants for Rhenium Thiozoline (thoz) versus Oxazoline (hoz) Complexes<sup>a</sup>

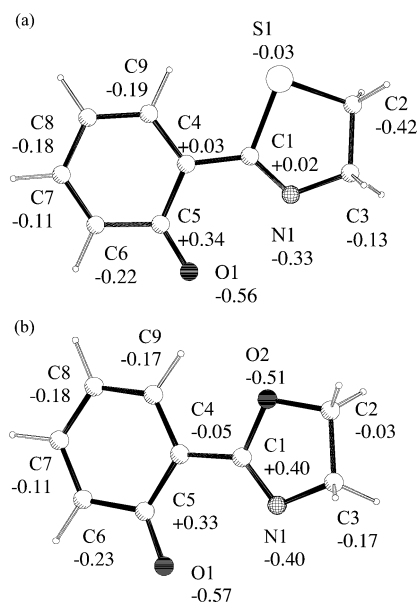
1. Oxo Transfer to Rhenium(V)			
reaction	L	rate constant	
		$K_1/M^{-1}$	$k_2/s^{-1}$
$(L)_2Re^V(O)^+ + PyO \rightarrow (L)_2Re^{VII}(O)_2^+ + Py$	hoz	$83 \pm 5$	$56 \pm 1$
	thoz	$32 \pm 2$	$46 \pm 1$
2. Oxo Transfer from Rhenium(VII) <sup>b</sup>			
reaction	L	$k_3/M^{-1} s^{-1}$	
$(L)_2Re(O)_2^+ + t-Bu_2S \rightarrow (L)_2Re(O)^+ + t-Bu_2S(O)$	hoz	$1482 \pm 79$	
	thoz	$27000 \pm 3000$	
$(L)_2Re(O)_2^+ + PhSMe \rightarrow (L)_2Re(O)^+ + PhS(O)Me$	hoz	$110 \pm 8$	
	thoz	$2300 \pm 250$	
3. Deactivation of Rhenium(VII) <sup>b</sup>			
reaction	L	$k_4/M^{-1} s^{-1}$	
$(L)_2Re(O)_2^+ + H_2O \rightarrow (L)Re(O)_3$	hoz	$(2.8 \pm 0.2) \times 10^{-4}$	
	thoz	$(5.0 \pm 0.3) \times 10^{-3}$	

<sup>a</sup> The rate constants were measured in acetonitrile at 293 K. <sup>b</sup> The kinetics determinations for the thiazoline complex were performed by sequential stopped-flow techniques.

**Table 6.** Bond Length Comparison between Complexes **1a**, **2**, and **6**<sup>a</sup>

	<b>1a</b>	<b>2</b> <sup>b</sup>	<b>6</b>
Re–N(1)	2.111(3)	2.035(8)	2.272(3)
N(1)–C(7)	1.292(13)	1.298(5)	1.286(4)
C(7)–S(1)/C(7)–O(5)	1.743(4)	1.359(11)	1.332(4)
C(8)–S(1)/C(8)–O(5)	1.795(6)	1.473(12)	1.470(4)

<sup>a</sup> The bond lengths are in angstroms. <sup>b</sup> From ref 46.


**Figure 9.** Charge distribution in the anionic ligands (a) hoz and (b) thoz.

the lower stability of the dioxorhenium(VII) thiazoline complex **4a** makes it the lesser catalyst of the two.

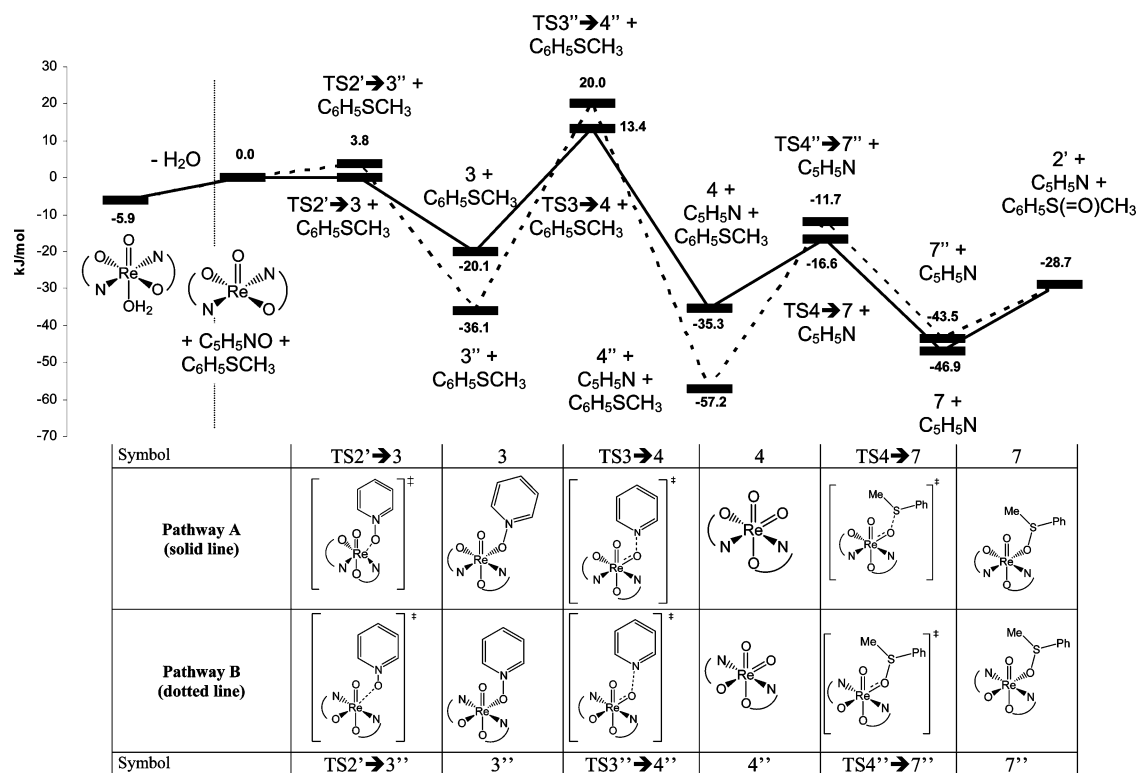
**Density Functional Theory (DFT) Calculations.** The oxidation of oxorhenium(V) oxazoline by pyridine *N*-oxide to give cationic dioxorhenium(VII) as well as the reduction of the latter by thioanisole, completing the catalytic cycle for OAT, were calculated using DFT methods. Details of the computational procedure are given in the Experimental Section. The full reaction pathway is shown in Scheme 4. The net OAT from PyO to PhSMe is exergonic by 28.7 kJ mol<sup>-1</sup>, which is an underestimate of  $\Delta G_{rxn} = -61$  kJ mol<sup>-1</sup>

based on enthalpic data for oxo transfer half-reactions (Tables 1 and 4). Two pathways that differ in the stereochemistry around rhenium were considered. Pathway A, indicated by the solid line in Scheme 4 includes all the intermediates and transition states with the nitrogen as well as oxygen atoms cis with respect to each other. On the basis of the molecular structure of complex **6** (Figure 6) and spectroscopic characterization of **4**,<sup>16</sup> pathway A is the experimentally prevalent reaction route. The dotted line represents pathway B, in which the nitrogen atoms of the hoz ligands are trans to each other.

The energies are given relative to the five-coordinate intermediate **2'** which is formed from the cationic rhenium(V) complex **2** (Figure 10a) with a weakly coordinated water molecule, as shown by a Re–O4 (water) distance of 2.49 Å. The bond length calculated for the hoz oxygen atoms O1 and O2 to the metal is in both cases 1.99 Å, revealing a Re–O single bond, while the 1.67 Å distance between Re and O3 (axial and trans to the water) indicates a Re–O double bond. The two nitrogen atoms from the hoz ligands (N1 and N2) coordinate to rhenium with bond lengths of 2.06 and 2.05 Å, respectively. The trans arrangement of the water ligand to O3 is thermodynamically more stable by 11.5 kJ/mol than the cis isomer (not shown). Indeed, the molecular structure of **2** features a trans aqua ligand to the Re=O multiple bond and trans hoz ligands in the equatorial plane.<sup>46</sup> Additionally, the calculated structure of complex **2** (bond lengths and angles) is in excellent agreement with the experimental X-ray structure. The dissociation of the water ligand is a slightly endergonic reaction (5.9 kJ/mol), leading to the formation of the distorted square-pyramidal complex **2'** (Figure 10b) with longer Re–N distances of 2.09 Å, while the oxygen atoms O1 and O2 consequently show shorter bonds of 1.91 Å to rhenium.

The preferred addition of the oxygen atom donor (in this case PyO) is cis to the Re=O bond of the intermediate **2'**, resulting in either the all-cis adduct **3** or the trans configuration of the oxazoline nitrogens in complex **3'** via the

Scheme 4



corresponding transition states  $\text{TS2}' \rightarrow 3$  and  $\text{TS2}' \rightarrow 3''$  (Figure 11). Transition state  $\text{TS2}' \rightarrow 3''$  shows only a small barrier of 3.8 kJ/mol, while the corresponding process via  $\text{TS2}' \rightarrow 3$  has no barrier. The structure given in Figure 11 for  $\text{TS2}' \rightarrow 3$  is only partially optimized with a constraint in the O4–Re distance. Different techniques to optimize the TS have been employed, but in all cases it was found to be a barrierless process. The Re–O4 distance shows a similar effect via pathway B with a rather long distance of 3.24 Å in  $\text{TS2}' \rightarrow 3''$  and 2.19 Å in the intermediate  $3''$ . The N3–O4 bond in PyO changes from 1.27 Å via 1.30 Å in the transition state to 1.34 Å in the adduct  $3''$ . While the adduct  $3''$  is favored thermodynamically over  $3$ , it has a larger activation energy toward oxo transfer and formation of  $4''$  (Scheme 4).

The addition of pyridine *N*-oxide to rhenium is a prior-equilibrium step, as the following step, oxo transfer to rhenium, is the rate determining step of the catalytic reaction (Scheme 4). This computational finding is in agreement with the experimental kinetic investigations (Scheme 2B). Even though complex  $4''$  is a thermodynamic sink, the calculations show that pathway A is favored kinetically by a factor of 14. In other words, the formation of  $4$  is favored by  $\Delta\Delta G^\ddagger = 6.6 \text{ kJ mol}^{-1}$  over  $4''$ . This estimate, however, does not concur with experimental findings, as the stereochemistry of  $4''$  is not observed. The transition states  $\text{TS3} \rightarrow 4$  and  $\text{TS3}'' \rightarrow 4''$  as well as the structures of the dioxorhenium(VII) stereoisomers  $4$  and  $4''$  are shown in Figure 12.

For pathway A, the Re–O4 distance decreases from 2.19 Å in adduct  $3$  over 1.82 Å in the transition state to 1.70 Å in the dioxo complex  $4$ , while the N3–O4 bond is 1.77 Å in the transition state  $\text{TS3} \rightarrow 4$ . For pathway B, a similar

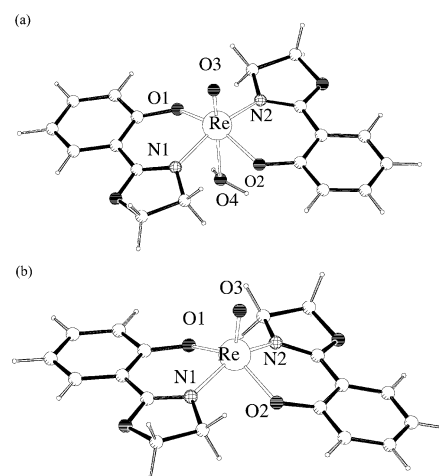


**Figure 10.** DFT optimized structures: (a) the rhenium(V) water complex **2** and (b) the five-coordinate intermediate **2'**.

picture evolves; the Re–O4 distance, which is the same in  $3''$  and  $3$ , decreases to 1.86 Å in the transition state  $\text{TS3}'' \rightarrow 4''$  and to 1.71 Å in the dioxo complex  $4''$ .

The second half of the catalytic cycle is the reduction of the cationic dioxorhenium(VII) complex  $4$  via addition of thioanisole and dissociation of the product phenylmethyl sulfoxide, thereby completing the catalytic cycle and regenerating the five-coordinate intermediate  $2'$ . Two pathways were considered for the reduction of stereoisomers  $4$  and  $4''$  (Scheme 4).

The all-cis dioxo complex  $4$  is the more active species with an activation energy of 18.7 kJ mol<sup>-1</sup> toward sulfoxide formation versus an activation barrier of 45.5 kJ mol<sup>-1</sup> for isomer  $4''$ . In the transition state  $\text{TS4} \rightarrow 7$ , the sulfur atom of thioanisole approaches O4 at 2.02 Å, compared to 1.97

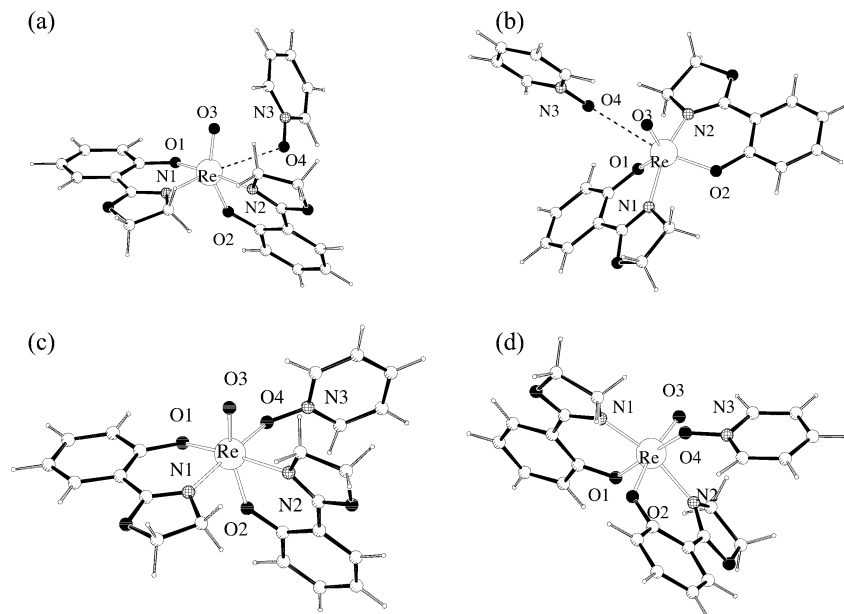


**Figure 11.** Transition states and intermediates for the addition of pyridine *N*-oxide: (a)  $\text{TS2}' \rightarrow 3$ , (b)  $\text{TS2}' \rightarrow 3''$ , (c) the all-cis adduct **3**, and (d) the N1–N2 trans adduct **3''**.

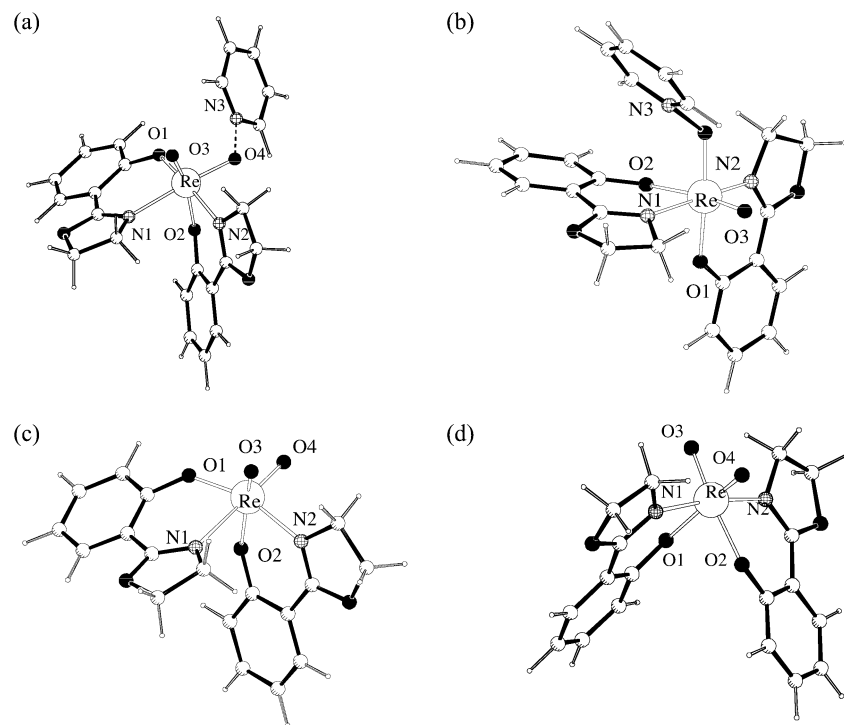


**Figure 12.** Transition states and dioxorhenium(VII) intermediates for the dissociation of pyridine: (a)  $\text{TS3} \rightarrow 4$ , (b)  $\text{TS3}'' \rightarrow 4''$ , (c) the all-cis dioxo complex **4**, and (d) the N1–N2 trans dioxo complex **4''**.

Å in  $\text{TS4}'' \rightarrow 7''$  (Figure 13). The Re–O4 bond is significantly elongated to 1.83 Å in  $\text{TS4} \rightarrow 7$  and 1.87 Å in  $\text{TS4}'' \rightarrow 7$ . The corresponding adduct **7** is exergonic by 11.6 kJ mol<sup>−1</sup>, while **7''** is only accessible from **4''** via an endergonic reaction (+13.7 kJ mol<sup>−1</sup>). The endergonic dissociation of phenylmethyl sulfoxide regenerates the catalytic species **2'** and closes the catalytic cycle. It is noteworthy that on the basis of a  $\Delta G^\circ$  value of −67 kJ mol<sup>−1</sup> for the half-reaction  $2 + \frac{1}{2}\text{O}_2 \rightarrow 4$ , a free energy of −66.3 kJ mol<sup>−1</sup> can be calculated for the oxo transfer half-reaction  $\text{PhSMe} + \frac{1}{2}\text{O}_2 \rightarrow \text{PhS(O)Me}$ , which is an underestimate by more than 20

kJ mol<sup>−1</sup> of the predicted value based on available enthalpic data (Table 4). This could be attributed to solvation effects as well as the level of theory employed.<sup>51</sup>

## Conclusion

Rhenium oxazoline and thiazoline complexes are versatile catalysts for a variety of OAT reactions. A testament to their remarkable activity is their ability to catalyze perchlorate reduction efficiently by pure oxo transfer, an extremely challenging reaction. The kinetics of oxo transfer from substrates to give a cationic dioxorhenium(VII) complex as

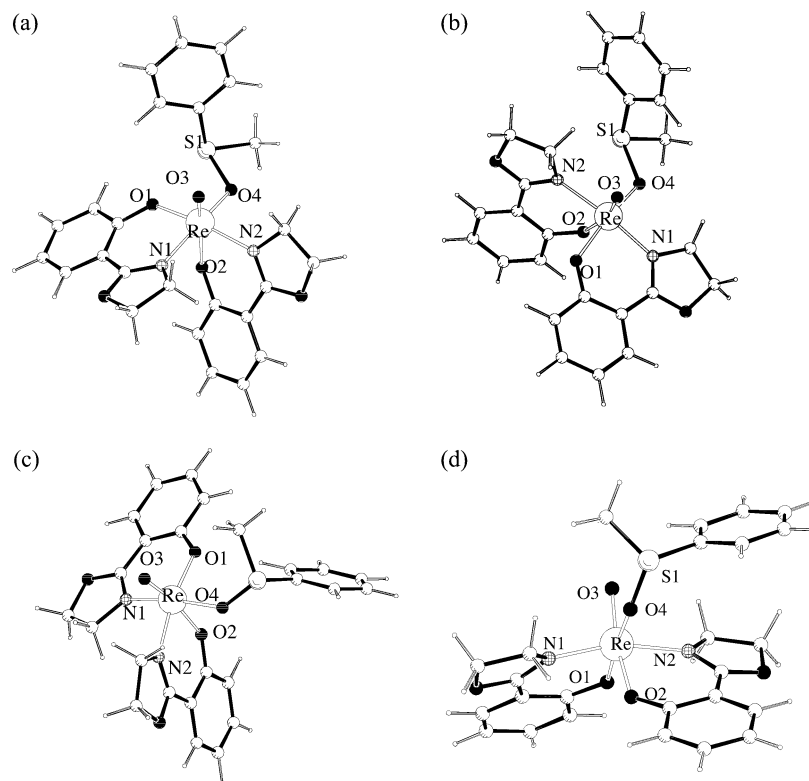
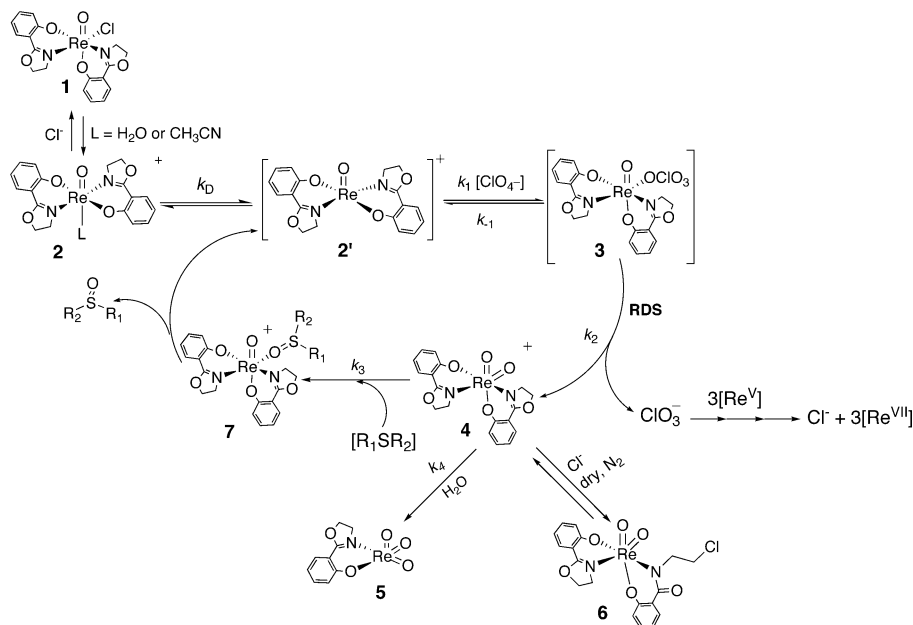


**Figure 13.** DFT-calculated structures for the addition of thioanisole to the dioxorhenium(VII) catalyst: (a)  $\text{TS4} \rightarrow 7$ , (b)  $\text{TS4}'' \rightarrow 7''$ , (c) the sulfoxido adduct **7**, and (d) the sulfoxido adduct  $7''$ .

#### Scheme 5



well as the kinetics from the latter to acceptor substrates are impressively fast approaching biological oxotransferase activity. For example, the turnover rates for perchlorate and pyridine *N*-oxide reduction by the rhenium(V) oxazoline catalyst **2** are 360 and  $2 \times 10^5 \text{ h}^{-1}$ , respectively. The latter is comparable to the enzymatic activity observed for trimethylamine *N*-oxide reductase and DMSO reductase.<sup>55,56</sup> All of the chemical transformations that have been fully characterized (chemically and kinetically) are summarized

in the catalytic cycle in Scheme 5 for the perchlorate reaction; similar mechanisms can be drawn for other oxo donors and acceptors. The RDS is the oxo transfer from the donor (XO) to form the dioxorhenium(VII) complex **4**.

Further insights into transition state structures along the reaction pathways have been sought by high-level density

(55) Buc, J.; Santini, C.-L.; Giordani, R.; Czjzek, M.; Wu, L.-F.; Giordani, G. *Mol. Microbiol.* **1999**, *32*, 159–168.

(56) Stewart, L. J.; Bailey, S.; Bennett, B.; Charnock, J. M.; Garner, C. D.; McAlpine, A. S. *J. Mol. Biol.* **2000**, *299*, 593–600.

functional theory (DFT) calculations. They allowed in this case the evaluation of the full catalytic cycle and identification of two reaction pathways. The oxygen atom transfer to rhenium(V) has been found to be the rate determining step, which is in agreement with experiment. In one of the calculated pathways, theory predicted the formation of a linkage isomer of the dioxorhenium(VII) complex **4''** (Scheme 4) as the thermodynamic product. Nevertheless, this isomer is not observed experimentally, and its stability must be an overestimate.

## Experimental Section

**Chemicals and Instrumentation.** All of the solvents were dried and distilled over CaH<sub>2</sub>. The reactions were carried out using standard Schlenk techniques. Hthoz (2-(2'-hydroxyphenyl)-2-thiazoline),<sup>57,58</sup> Re(O)Cl<sub>3</sub>(PPh<sub>3</sub>)<sub>2</sub>,<sup>59</sup> Re(O)Cl<sub>3</sub>(OPPh<sub>3</sub>)(SMe<sub>2</sub>),<sup>60</sup> and [Bu<sub>4</sub>N][ReOCl<sub>4</sub>]<sup>61</sup> were prepared according to previously published methods. The NMR spectra were obtained on Bruker AC200, ARX400, and ARX500 spectrometers. The UV-vis spectra were recorded on a Shimadzu UV-2501 spectrophotometer. The stopped-flow kinetics were collected on an Applied Photophysics SX.18MV stopped-flow reaction analyzer. The time profiles were analyzed with the KaleidaGraph 3.0 program on a Macintosh or PC.

**Chlorobis[2-(2'-hydroxyphenyl)-2-oxazoline]oxorhenium(V), ReO(hoz)<sub>2</sub>Cl (1).** *Procedure 1—High Yield.* The ligand Hhoz (280 mg, 1.72 mmol) was dissolved in ethanol (30 mL, 200 proof) followed by 2,6-lutidine (0.50 mL, 1.72 mmol). Re(O)Cl<sub>3</sub>(OPPh<sub>3</sub>)(SMe<sub>2</sub>) (510 mg, 0.786 mmol) was added to the flask after 5 min. The light green suspension was refluxed for 3 h under an ambient atmosphere. Once the solution cooled to room temperature, the dark green precipitate was filtered, thoroughly washed with diethyl ether, and dried (351 mg, 80% yield). <sup>1</sup>H NMR (CD<sub>2</sub>Cl<sub>2</sub>, 25 °C): δ 7.93 (d, *J* = 6.5 Hz, 1H), 7.68 (d, *J* = 6.3 Hz, 1H), 7.45 (t, *J* = 6 Hz, 1H), 7.20 (t, *J* = 6 Hz, 1H), 6.96 (t, 1H), 6.87 (d, *J* = 7.8 Hz, 1H), 6.81 (t, 1H), 6.75 (d, *J* = 8.4 Hz, 1H), 5.05 (q, *J* = 8.9 Hz, 1H), 4.97 (t, *J* = 7.0 Hz, 2H), 4.85 (q, *J* = 8.9 Hz, 1H), 4.72 (t, *J* = 9.0 Hz, 2 H), 4.20 (m, 2H). EI<sup>+</sup>-MS: *m/z* calculated for C<sub>18</sub>ClH<sub>16</sub>N<sub>2</sub>O<sub>5</sub>Re (M<sup>+</sup>), 561.844; found, 562. Anal. Calcd for C<sub>18</sub>ClH<sub>16</sub>N<sub>2</sub>O<sub>5</sub>Re: C, 38.5; H, 2.9; N, 5.0. Found: C, 38.2; H, 2.8; N, 5.0.

**Chlorobis[2-(2'-hydroxyphenyl)-2-oxazoline]oxorhenium(V), ReO(hoz)<sub>2</sub>Cl (1).** *Procedure 2—Fast Preparation.* The procedure outlined above was followed using Re(O)Cl<sub>3</sub>(PPh<sub>3</sub>)<sub>2</sub> (500 mg, 0.60 mmol), Hhoz ligand (294 mg, 1.80 mmol), and 2,6-lutidine (450 μL, 1.80 mmol). The yield of **1** was 150 mg (45%).

**2-(2'-Hydroxyphenyl)-2-thiazoline, Hthoz.** To a stirred solution of 2-hydroxybenzoxazole (1.00 g, 8.39 mmol, Lancaster) in 30 mL of methanol was added cysteamine (1.19 g, 16.8 mmol, Fluka). The solution was refluxed for 5 h under an argon atmosphere after which the solvent was removed under vacuum. The orange residue was extracted with 70 mL of Et<sub>2</sub>O and the extract passed through

a column (200–400 mesh Silica gel) using pentane/Et<sub>2</sub>O (9:1). The quickly eluting yellow band was collected and dried under vacuum to yield a yellow powder, Hthoz (0.52 g, 35% yield). <sup>1</sup>H NMR (CDCl<sub>3</sub>, 25 °C): δ 12.14 (s, 1H), 7.38 (m, 2H), 6.99 (d, 1H), 6.87 (t, 1H), 4.47 (t, 2H), 3.36 (t, 2H).

**Chlorobis[2-(2'-hydroxyphenyl)-2-thiazoline]oxorhenium(V), ReO(hoz)<sub>2</sub>Cl (1a).** To a stirred solution of Hthoz (153 mg, 0.838 mmol) in 20 mL of ethanol was added 2,6-lutidine (0.1 mL). After 5 min, [Bu<sub>4</sub>N][ReOCl<sub>4</sub>] (250 mg, 0.427 mmol) was added to the solution. After 20 min. a dark green precipitate was filtered out and washed with cold EtOH and pentane. The powder was recrystallized at -10 °C using CH<sub>2</sub>Cl<sub>2</sub>/pentane to achieve dark green crystals (50.4 mg, 33% yield). <sup>1</sup>H NMR (CD<sub>2</sub>Cl<sub>2</sub>, 25 °C): δ 7.73 (d, 1H), 7.58 (d, 1H), 7.44 (t, 1H), 7.21 (t, 1H), 6.98 (t, 1H), 6.78 (m, 3H), 5.47 (m, 1H), 5.03 (m, 1H), 4.54 (m, 1H), 4.39 (m, 1H), 3.87 (q, 1H), 3.73 (m, 2H), 3.60 (q, 1H). EI<sup>+</sup>-MS: *m/z* calculated for C<sub>18</sub>ClH<sub>16</sub>N<sub>2</sub>O<sub>3</sub>S<sub>2</sub>Re (M<sup>+</sup>), 593.984; found, 594.0. Anal. Calcd for C<sub>18</sub>ClH<sub>16</sub>N<sub>2</sub>ReO<sub>3</sub>S<sub>2</sub>: C, 36.4; H, 2.72; N, 4.72; S, 10.8. Found: C, 36.5; H, 2.69; N, 4.87; S, 10.6.

**Bis[2-(2'-hydroxyphenyl)-2-oxazoline]oxorhenium(V) Trifluoromethanesulfonate, [ReO(hoz)<sub>2</sub>][OTf] (2).** To a stirred solution of **1** (203 mg, 0.362 mmol) in 30 mL of CH<sub>3</sub>CN was added AgOTf (102 mg, 0.397 mmol). After refluxing for 1 h, the precipitate was filtered out when cool and the solvent was removed by rotovap. The residue was recrystallized with CH<sub>2</sub>Cl<sub>2</sub>/pentane to yield a dark green powder (233 mg, 95%). <sup>1</sup>H NMR (CD<sub>2</sub>Cl<sub>2</sub>, 25 °C): δ 7.98 (d, *J* = 8.0 Hz, 2H), 7.60 (t, *J* = 7.7 Hz, 2H), 7.19 (d, *J* = 7.4 Hz, 2H), 6.95 (t, *J* = 8.4 Hz, 2H), 4.95 (m, 6H), 4.38 (m, 2H). <sup>19</sup>F NMR (CD<sub>2</sub>Cl<sub>2</sub>, 25 °C): δ -79.86. EI<sup>+</sup>-MS: *m/z* calculated for C<sub>19</sub>F<sub>3</sub>H<sub>16</sub>N<sub>2</sub>O<sub>8</sub>S<sub>1</sub>Re (M<sup>+</sup>), 675.608; found, 676.0. Anal. Calcd for C<sub>19</sub>F<sub>3</sub>H<sub>16</sub>N<sub>2</sub>O<sub>8</sub>ReS: C, 33.8; H, 2.4; N, 4.1; S, 4.7. Found: C, 32.6; H, 2.4; N, 4.2; S, 4.5.

**Bis[2-(2'-hydroxyphenyl)-2-thiazoline]oxorhenium(V) Trifluoromethanesulfonate, [ReO(hoz)<sub>2</sub>][OTf] (2a).** To a stirred solution of **1a** (50.4 mg, 0.0850 mmol) in 30 mL of CH<sub>3</sub>CN was added AgOTf (21.8 mg, 0.0850 mmol). After stirring for 1 h at room temperature, the precipitate was filtered out and the solvent was removed by rotovap. The residue was recrystallized with CH<sub>2</sub>Cl<sub>2</sub>/pentane to yield an olive green powder (45 mg, 60%). <sup>1</sup>H NMR (CD<sub>2</sub>Cl<sub>2</sub>, 25 °C): δ 7.81 (d, *J* = 8.0 Hz, 2H), 7.46 (t, *J* = 7.7 Hz, 2H), 6.98 (t, 2H), 6.91 (d, 2H), 5.02 (q, 2H), 4.90 (q, 2H), 4.49 (q, 2H), 4.21 (q, 2H). <sup>19</sup>F NMR (CD<sub>2</sub>Cl<sub>2</sub>, 25 °C): δ -79.86. EI<sup>+</sup>-MS: *m/z* calculated for C<sub>19</sub>F<sub>3</sub>H<sub>16</sub>N<sub>2</sub>O<sub>6</sub>S<sub>3</sub>Re (M<sup>+</sup>), 707.968; found, 708.0.

**[N-(2-Chloroethyl)-1-(2'-hydroxyphenyl)methamidato][2-(2'-hydroxyphenyl)-2-oxazoline]dioxorhenium(VII) (6).** To a solution of **1** (30 mg, 0.0534 mmol) in 60 mL of CH<sub>3</sub>CN was added pyridine *N*-oxide (5.1 mg, 0.0537 mmol). The solution was allowed to stir for 3 h until the color changed to brown. The solvent was reduced under vacuum to ~1 mL in volume and transferred to an NMR tube. The tube was sealed and stored at -20 °C for 2 days until brown crystals formed. MALDI<sup>-</sup>-MS: *m/z* calculated for C<sub>18</sub>-ClH<sub>16</sub>N<sub>2</sub>O<sub>6</sub>Re (M<sup>-</sup>), 578.07; found, 578.06. Anal. Calcd for C<sub>18</sub>-ClH<sub>16</sub>N<sub>2</sub>O<sub>6</sub>Re: C, 37.40; H, 2.79; N, 4.85. Found: C, 37.60; H, 2.83; N, 4.86.

**X-ray Structure Determinations.** A green parallelepiped of **1a** and a black prism of **6** with approximate dimensions of 0.3 × 0.4 × 0.6 mm<sup>3</sup> and 0.30 × 0.35 × 0.40 mm<sup>3</sup>, respectively, were used for the X-ray crystallographic analyses. The X-ray intensity data were measured at 297 K for **1a** and at 100 K for **6** on a Bruker Smart 1000 CCD-based X-ray diffractometer system equipped with a Mo-target X-ray tube (λ = 0.710 73 Å) operated at 2250 W of power. The detector was placed at a distance of 4.986 cm from the crystal.

(57) Nishiyama, H.; Yamaguchi, S.; Kondo, M.; Itoh, K. *J. Org. Chem.* **1992**, *57*, 4306–4309.

(58) Hoveyda, H. R.; Rettig, S. J.; Orvig, C. *Inorg. Chem.* **1992**, *31*, 5408–5416.

(59) Parshall, G. W. *Inorg. Synth.* **1977**, *17*, 110.

(60) Grove, D. E.; Wilkinson, G. J. *J. Chem. Soc. A* **1966**, 1224.

(61) Alberto, R.; Schibli, R.; Egli, A.; Schubinger, P. A.; Herrmann, W. A.; Artus, G.; Abram, U.; Kaden, T. A. *J. Organomet. Chem.* **1995**, *492*, 217–224.

A total of 1321 frames were collected with a scan width of 0.3° in  $\omega$ , with an exposure time of 30 s per frame. The total data collection time was 18.6 h. The frames were integrated with the Bruker Saint Software package using a narrow-frame integration algorithm. The integration of data using a monoclinic cell for **1a** and a triclinic cell for **6** yielded a total of 12 412 ( $\theta_{\max} = 28.31$ ) and 5841 ( $\theta_{\max} = 28.27$ ) reflections of which 4669 and 4048 were independent reflections, respectively. The final cell constants (**1a**:  $a = 16.352(2)$  Å,  $b = 7.6666(8)$  Å,  $c = 16.513(2)$  Å,  $\beta = 111.108(2)^\circ$ ,  $V = 1931.2(4)$  Å<sup>3</sup>. **6**:  $a = 9.388(1)$  Å,  $b = 9.973(1)$  Å,  $c = 10.968(2)$  Å,  $\alpha = 101.743(2)^\circ$ ,  $\beta = 111.077(2)^\circ$ ,  $\gamma = 103.221(3)^\circ$ ,  $V = 885.5(2)$  Å<sup>3</sup>) are based upon the refinement of the *xyz* centroids of 1024 reflections.

The structure was refined with the Bruker Shelxtl Software package, using the space group  $P2_1/n$  with  $Z = 4$  and  $P\bar{1}$  with  $Z = 2$  for **1a** and **6**, respectively. The final anisotropic full-matrix least-squares refinement on  $F^2$  converged at  $R1 = 0.039$  and  $wR2 = 0.106$  for **1a** and  $R1 = 0.023$  and  $wR2 = 0.061$  for **6**.

**Stopped-Flow Kinetics with 2 and 2a under Non-Steady-State Conditions.** Solutions of **2** (or **2a**) were prepared in acetonitrile (0.50 mM) and reacted with an oxidant in excess concentrations (5.0–200 mM) to achieve pseudo-first-order conditions. The reactions with perchlorate and chlorate were conducted in a 95:5 CH<sub>3</sub>CN/H<sub>2</sub>O solvent system. The reactions with the PyO substrates and *t*-BuOOH were carried out in CH<sub>3</sub>CN. The increase in absorbance from the dioxorhenium(VII) species produced was monitored at 500 nm by stopped-flow spectrophotometry. Plots of the pseudo-first-order rate constant ( $k_p$ ) versus [oxidant] showed saturation dependence. Fits of the data to the appropriate rate law yielded a first-order rate constant ( $k_2$ ) and an equilibrium constant ( $K_1$ ) for each of the oxidants used.

**Stopped-Flow Kinetics with 4 and 4a under Non-Steady-State Conditions.** A solution of the oxidized form of **2** or **2a**, the dioxorhenium(VII) complex, was prepared by adding a stoichiometric amount of 4-picoline *N*-oxide (0.50 mM) to **2** or **2a** (0.50 mM) in acetonitrile at 25 °C. The reaction was followed to completion by UV–vis at 500 nm, where **4** and **4a** absorb exclusively. The solution was used immediately after preparation. Complex **4** or **4a** was then reduced in situ with excess organic sulfide (4.0–90.0 mM) to achieve pseudo-first-order conditions. The decay of the absorbance at 500 nm was monitored by stopped-flow. A plot of the pseudo-first-order rate constants ( $k_p$ 's) versus thioether concentration was linear, and the slope afforded a second-order rate constant ( $k_3$ ).

**Temperature Dependence of Oxidation Kinetics.** Solutions of **2** were prepared in acetonitrile (0.50 mM) and reacted with an oxidant at a concentration that gives saturation kinetics, [picoline *N*-oxide] = 0.109 M and [ClO<sub>3</sub><sup>-</sup>] = 6.76 mM. The temperatures of the reagents and the stopped-flow reaction cell were changed for each run from 5 to 40 °C. The increase in absorbance from the dioxorhenium(VII) species produced was monitored at 500 nm by stopped-flow UV–vis spectrophotometry. Each trial gave a pseudo-first-order trace that yielded  $k_2$ . Arrhenius plots yielded  $\Delta H^\ddagger$ ,  $\Delta S^\ddagger$ ,  $E_a$ , and  $A$  for each oxidant.

**Computational Details.** All the calculations were performed with the Gaussian98 program.<sup>62</sup> The density functional hybrid model B3LYP<sup>63–66</sup> was used together with the 6-31G\*<sup>67–70</sup> basis set for C, H, N, O, and S. The Re basis set consists of a LANL2DZ basis set of double- $\zeta$  quality and a Hay and Wadt basis set<sup>71–73</sup> for the valence and penultimate shells, with an effective core potential (ECP) at rhenium.

No symmetry or internal coordinate constraints were applied during the optimizations. All reported intermediates were verified as true minima by the absence of negative eigenvalues in the vibrational frequency analysis. Transition state structures (indicated by **TS**) were located using the Berny algorithm<sup>74</sup> until the Hessian matrix had only one imaginary eigenvalue. The identities of all the transition states were confirmed by animating the negative eigenvector coordinate with a visualization program.

The approximate free energies were obtained through thermochemical analysis of the frequency calculation, using the thermal correction to Gibbs free energy as reported by Gaussian98. This takes into account zero-point effects, thermal enthalpy corrections, and entropy. All energies reported in this paper, unless otherwise noted, are free energies at 298 K, using unscaled frequencies. All the transition states are maxima on the electronic potential energy surface. These may not correspond to maxima on the free energy surface.

**Acknowledgment.** We thank the NSF (CHE-0208682 to M.M.A.O.), the Beckman Foundation (BYI award to M.M.A.O.), and the Bavarian-Californian Technology Fund (BaCaTec) for financial support of this research as well as the Leibniz-Rechenzentrum München for computer time. M.M.A.O. is grateful to Professor Jim Mayer for helpful discussion and comments on this manuscript.

**Supporting Information Available:** X-ray crystallographic data for **1a** and **6** (CIF), thermodynamic calculations (PDF), as well as the coordinates, structures, and energies from DFT calculations of compounds, intermediates, and transition states (PDF). This material is available free of charge via the Internet at <http://pubs.acs.org>.

IC0498945

- (62) Frisch, M. J.; Trucks, G. W.; Schlegel, H. B.; Scuseria, G. E.; Robb, M. A.; Cheeseman, J. R.; Zakrzewski, V. G.; Montgomery, J. A.; Stratmann, R. E.; Burant, J. C.; Dapprich, S.; Millam, J. M.; Daniels, A. D.; Kudin, K. N.; Strain, M. C.; Farkas, O.; Tomasi, J.; Barone, V.; Cossi, M.; Cammi, R.; Mennucci, B.; Pomelli, C.; Adamo, C.; Clifford, S.; Ochterski, J.; Petersson, G. A.; Ayala, P. Y.; Cui, Q.; Morokuma, K.; Malick, D. K.; Rabuck, A. D.; Raghavachari, K.; Foresman, J. B.; Cioslowski, J.; Ortiz, J. V.; Baboul, A. G.; Stefanov, B. B.; Liu, G.; Liashenko, A.; Piskorz, P.; Komaromi, I.; Gomperts, R.; Martin, R. L.; Fox, D. J.; Keith, T.; Al-Laham, M. A.; Peng, C. Y.; Nanayakkara, A.; Gonzalez, C.; Challacombe, M.; Gill, P. M. W.; Johnson, B.; Chen, W.; Wong, M. W.; Andres, J. L.; Gonzalez, C.; Head-Gordon, M.; Replogle, E. S.; Pople, J. A. *Gaussian 98*, revision A.7; Gaussian, Inc.: Pittsburgh, PA, 1998.
- (63) Lee, C.; Yang, W.; Parr, R. G. *Phys. Rev. B: Condens. Matter Mater. Phys.* **1988**, *37*, 785–789.
- (64) Vosko, S. H.; Wilk, L.; Nusair, M. *Can. J. Phys.* **1980**, *58*, 1200–1211.
- (65) Stephens, P. J.; Devlin, F. J.; Chabalowski, C. F.; Frisch, M. J. *J. Phys. Chem.* **1994**, *98*, 11623–11627.
- (66) Becke, A. D. *J. Chem. Phys.* **1993**, *98*, 5648–5652.
- (67) Ditchfield, R.; Hehre, W. J.; Pople, J. A. *J. Chem. Phys.* **1971**, *54*, 724–728.
- (68) Hehre, W. J.; Ditchfield, R.; Pople, J. A. *J. Chem. Phys.* **1972**, *56*, 2257–2261.
- (69) Hariharan, P. C.; Pople, J. A. *Theor. Chim. Acta* **1973**, *28*, 213–222.
- (70) Hariharan, P.; Pople, J. A. *Mol. Phys.* **1974**, *27*, 209–214.
- (71) Hay, P. J.; Wadt, W. R. *J. Chem. Phys.* **1985**, *82*, 270–283.
- (72) Hay, P. J.; Wadt, W. R. *J. Chem. Phys.* **1985**, *82*, 284–298.
- (73) Hay, P. J.; Wadt, W. R. *J. Chem. Phys.* **1985**, *82*, 299–310.
- (74) Schlegel, H. B. *J. Comput. Chem.* **1982**, *3*, 214–218.